Acta Pharmaceutica Sinica B 2026;16(4):2396−2419

Chinese Pharmaceutical Association
Institute of Materia Medica, Chinese Academy of Medical Sciences

Acta Pharmaceutica Sinica B

www.elsevier.com/locate/apsb
www.sciencedirect.com

ORIGINAL ARTICLE

A neurotensin receptor type 1-derived pepducin acts as a biased allosteric modulator to regulate target receptor function

Rebecca L. Brouillette[a,b], Frédérique Lussier[a,b], Émile Breault[a,b], Nathan Meneboo[a,b], Malihe Hassanzadeh[a,b], Victoria Tremblay[a,b], Magali Chartier[a,b], Élora Midavaine[a,b], Laurence Ulrich[a,b], Jérôme Côté[a,b], Véronique Blais[a,b], Christine E. Mona[c,d], Jean-Michel Longpré[a,b], Michel Grandbois[a,b], Pierre-Luc Boudreault[a,b,e], Martin Audet[a,b], Élie Besserer-Offroy[a,e,f,g,*], Philippe Sarret[a,b,e,*]

[a]*Department of Pharmacology-Physiology, Faculty of Medicine and Health Sciences, Université de Sherbrooke, Sherbrooke, QC, J1H 5N4, Canada*
[b]*Institut de Pharmacologie de Sherbrooke, Université de Sherbrooke, Sherbrooke, QC, J1H 5N4, Canada*
[c]*Ahmanson Translational Theranostics Division, Department of Molecular and Medical Pharmacology, David Geffen School of Medicine, University of California-Los Angeles, Los Angeles, CA 90095, USA*
[d]*Jonsson Comprehensive Cancer Center, UCLA Health, Los Angeles, CA 90095, USA*
[e]*RECITAL International Partnership Lab, Université de Caen Normandie, 14000, Caen, France & Université de Sherbrooke, QC, J1H 5N4, Canada*
[f]*Interdisciplinary Research Unit for Cancer Prevention and Treatment − Anticipe, INSERM, U1086, Université de Caen Normandie, 14000 Caen, France*
[g]*François Baclesse Comprehensive Cancer Center, UNICANCER, 14000 Caen, France*

Received 1 August 2025; received in revised form 12 November 2025; accepted 4 December 2025

KEY WORDS

Pepducin;
Lipopeptide;
Neurotensin receptor type

Abstract Pepducins are synthetic membrane-tethered lipopeptides designed to allosterically modulate G protein-coupled receptor (GPCR) signaling. Here, we characterize a series of pepducins targeting the neurotensin receptor type 1 (NTSR1), revealing their complex and multifaceted modulation properties. Using BRET-based biosensors, we show that PP-001, a pepducin derived from NTSR1's first intracellular

*Corresponding authors.
E-mail addresses: elie.besserer-offroy@unicaen.fr (Élie Besserer-Offroy), philippe.sarret@usherbrooke.ca (Philippe Sarret).

Peer review under the responsibility of Chinese Pharmaceutical Association and Institute of Materia Medica, Chinese Academy of Medical Sciences.

https://doi.org/10.1016/j.apsb.2025.12.043

1 (NTSR1);
G protein-coupled receptor (GPCR);
Biased agonism;
Allostery;
Drug discovery

loop, preferentially activates G protein over β-arrestin signaling while inhibiting NT binding, NT-induced β-arrestin recruitment, and NTSR1 internalization, thereby acting as biased allosteric agonist and negative allosteric modulator. PP-001 also promotes the formation of both homo- and heteromeric multi-receptor complexes. *In vivo*, PP-001 elicits potent, sustained hypotensive effects, reversible by the NTSR1 antagonist SR48692. Although the precise mechanism of pepducin-receptor interaction remains unclear, we identify a critical N-terminal RKK motif for PP-001's biological activity. Finally, thermodenaturation assays using purified NTSR1, combined with mutagenesis and molecular docking, provide evidence for the role of the receptor's H8 domain in direct pepducin interaction. Together, these findings highlight pepducins as versatile modulators of GPCR function and as valuable pharmacological tools for GPCR-targeted drug development.

1. Introduction

Pepducins represent a unique class of drugs designed to target G protein-coupled receptors (GPCRs), also known as 7-transmembrane domain receptors (7TMRs), by using a distinctive intracellular allosteric mechanism. Structurally, pepducins consist of a lipid moiety, most commonly palmitate, conjugated to a peptide derived from one of the four intracellular domains (ICLs 1−3, C-terminus) of a receptor of interest[1]. Functionally, the lipid serves as a tether to the cell membrane's phospholipid bilayer and allows the pepducin's passive translocation between the outer and inner leaflets[2,3]. Once the pepducin penetrates the intracellular compartment, it is thought to allosterically bind to its cognate receptor and thereby modulate the signaling output[4]. However, the nature of this modulation may be multifarious. Some pepducins have been reported to directly promote 7TMR signaling and could thus be classified as allosteric agonists[5−7]. Others have been shown to inhibit the activity of an extracellular agonist, behaving as negative allosteric modulators (NAMs) of their target receptor[8−10]. Conceivably, they could also potentiate the activity of an extracellular agonist and behave as positive allosteric modulators (PAMs) of their receptor, although no examples of pepducins acting in this way have been reported. A small number of pepducins are also known to inhibit responses triggered by other (agonistic) pepducins[11,12]. Importantly, these lipopeptides can display signaling bias by preferentially activating (or inhibiting) a subset of the receptor's associated signaling pathways, unlike a balanced reference ligand[6,7,13]. Finally, due to their unique mode of action, pepducins may regulate receptor function in ways that are simply not possible with traditional ligands[14]. In short, they have the potential to be very useful tools in drug discovery, for both research and therapeutic purposes.

To date, pepducins have been derived from a range of 7TMRs, including protease-activated receptors 1, 2, and 4 (PAR1, PAR2, and PAR4)[1,15]; chemokine receptors CCR2[16], CXCR1/2[17,18], and CXCR4[5,17]; β2 adrenergic receptor (β2R)[6,7]; formyl peptide receptors 1, 2, and 3 (FPR1[19], FPR2[20,21], and FPR3[22]); sphingosine-1-phosphate receptors S1PR1 and S1PR3[12,23]; and urotensin receptor (UTR)[24]. With such a varied list of targets, the pathophysiological contexts in which pepducins have been studied are equally diverse: arthritis[25], cancer (breast[26], intestinal[27,28], lung[8,29], ovarian[18,30], prostate[31], and leukemia[32]), heart failure[33], dermatitis and itch[34,35], diabetes[36], liver disease[37], sepsis[17,38], and thrombosis[39,40], to name a few. Among them, PZ-128, a PAR1-derived pepducin, has successfully completed Phase I[41] and Phase II[39] clinical trials, and may thus become a first-of-its class drug on the market. Despite these advances, many questions remain about pepducins, including the precise nature of the pepducin−receptor interaction, which is still unclear. Thus, there is a need to deepen our mechanistic understanding of how these lipopeptides operate and to broaden our set of available tools by applying the pepducin strategy to new targets.

To this end, we recently introduced a new series of pepducins derived from the ICL1 of the neurotensin receptor type 1 (NTSR1), one of the two 7TMRs bound by the neurotensin tridecapeptide (NT)[42]. This Class A GPCR, expressed in central[43] and peripheral[44,45] tissues, mediates diverse physiological effects, including hypotension[46] and hypothermia[47]. Of particular interest, NTSR1 activation contributes to NT-induced opioid-independent analgesia in rodents[48−50]. Prior to our work, NTSR1 had not been targeted by pepducin technology, and research into the therapeutic potential of pepducins in chronic pain paradigms was limited. We recently demonstrated that the pepducin PP-001 derived from ICL1 exerted significant analgesic effects across multiple pain models[42]. In the present study, we aim to characterize in depth the signaling profile of PP-001 at NTSR1 and to elucidate the molecular basis of pepducin-receptor interactions. Our results reveal complex modulation of NTSR1 signaling, as PP-001 was found to behave as a biased allosteric agonist, favoring G protein signaling over β-arrestin recruitment, and as a negative allosteric modulator, reducing NT binding and signaling. Alanine scanning mutagenesis of both PP-001 and NTSR1's ICL domains also identifies key structural determinants governing this interaction. In particular, we found that the N-terminal RKK motif of PP-001 plays a critical role for its biological activity while the receptor's eighth α-helix (H8) constitutes a critical interface mediating pepducin-receptor interaction. Finally, thermodenaturation assays using purified NTSR1 receptor constructs, combined with molecular docking, provide direct evidence of PP-001 binding to NTSR1.

2. Materials and methods

2.1. Materials

To perform the experiments described here, we synthesized the compounds NT, NT(8-13), and our NTSR1-derived pepducins at the peptide synthesis facility of the Université de Sherbrooke (http://www.usherbrooke.ca/ips/en/platforms/psp/). These include the full-length ICL1 pepducin (NTSR1-ICL1-PP-001), a non-palmitoylated control (NTSR1-ICL1-NP-001), a pepducin with a

Table 1 Peptide sequences of tested compounds.

Compound	Abbreviation	Sequence
Neurotensin	NT	H_2N- E L Y E N K P R R P Y I L $-COOH$
Neurotensin (8-13)	NT(8-13)	H_2N- R R P Y I L $-COOH$
NTSR1-ICL1-PP-001	PP-001	Palmitoyl$-$ A R K K S L Q S L Q S T V H $-CO-NH_2$
NTSR1-ICL1-NP-001	NP-001	H_2N- A R K K S L Q S L Q S T V H $-CO-NH_2$
NTSR1-ICL1-PP-SCR-001	PP-SCR-001	Palmitoyl$-$ L V Q R L T A K S S K Q H S$-CO-NH_2$
NTSR1-ICL1-PP-005	PP-005	Palmitoyl$-$ A R K K S L $-CO-NH_2$
NTSR1-ICL1-[Ala^2]PP-001	[Ala^2]PP-001	Palmitoyl$-$ A A K K S L Q S L Q S T V H $-CO-NH_2$
NTSR1-ICL1-[Ala^3]PP-001	[Ala^3]PP-001	Palmitoyl$-$ A R A K S L Q S L Q S T V H $-CO-NH_2$
NTSR1-ICL1-[Ala^4]PP-001	[Ala^4]PP-001	Palmitoyl$-$ A R K A S L Q S L Q S T V H $-CO-NH_2$
NTSR1-ICL1-[Ala^5]PP-001	[Ala^5]PP-001	Palmitoyl$-$ A R K K A L Q S L Q S T V H $-CO-NH_2$
NTSR1-ICL1-[Ala^6]PP-001	[Ala^6]PP-001	Palmitoyl$-$ A R K K S A Q S L Q S T V H $-CO-NH_2$
NTSR1-ICL1-[Ala^7]PP-001	[Ala^7]PP-001	Palmitoyl$-$ A R K K S L A S L Q S T V H $-CO-NH_2$
NTSR1-ICL1-[Ala^8]PP-001	[Ala^8]PP-001	Palmitoyl$-$ A R K K S L Q A L Q S T V H $-CO-NH_2$
NTSR1-ICL1-[Ala^9]PP-001	[Ala^9]PP-001	Palmitoyl$-$ A R K K S L Q S A Q S T V H $-CO-NH_2$
NTSR1-ICL1-[Ala^{10}]PP-001	[Ala^{10}]PP-001	Palmitoyl$-$ A R K K S L Q S L A S T V H $-CO-NH_2$
NTSR1-ICL1-[Ala^{11}]PP-001	[Ala^{11}]PP-001	Palmitoyl$-$ A R K K S L Q S L Q A T V H $-CO-NH_2$
NTSR1-ICL1-[Ala^{12}]PP-001	[Ala^{12}]PP-001	Palmitoyl$-$ A R K K S L Q S L Q S A V H $-CO-NH_2$
NTSR1-ICL1-[Ala^{13}]PP-001	[Ala^{13}]PP-001	Palmitoyl$-$ A R K K S L Q S L Q S T A H $-CO-NH_2$
NTSR1-ICL1-[Ala^{14}]PP-001	[Ala^{14}]PP-001	Palmitoyl$-$ A R K K S L Q S L Q S T V A $-CO-NH_2$

scrambled peptide sequence (NTSR1-ICL1-PP-SCR-001), a C-terminally truncated pepducin (NTSR1-ICL1-PP-005), and a 13-pepducin alanine scan series in which the amino acids at positions 2 to 14 of NTSR1-ICL1-PP-001 (corresponding to residues R90 to H102 of hNTSR1) have been sequentially replaced by alanine residues (NTSR1-ICL1-[Ala^2]PP-001 to NTSR1-ICL1-[Ala^{14}]PP-001). We also obtained the NTSR1 antagonist SR48692 from R&D Systems, Inc. (Minneapolis, MN, USA). The specific peptide sequences are provided in Table 1.

Throughout this article, pepducins are referred to by their abbreviated titles PP-001, NP-001, PP-SCR-001, etc. The protected amino acids and TentaGel R-RAM resins used in their synthesis were obtained from Chem-Impex International (Wood Dale, IL, USA). All other chemicals and reagents involved in the synthesis of peptides and pepducins were obtained from Sigma-Aldrich (Oakville, ON, Canada) or Fisher Scientific (Montreal, QC, Canada). Dulbecco's modified Eagle's medium (DMEM): Nutrient Mixture F12 (DMEM-F12), Leibovitz (L-15) medium, HEPES (4-(2-hydroxyethyl)-1-piperazineethanesulfonic acid), penicillin−streptomycin, fetal bovine serum (FBS), gentamycin G418, phosphate-buffered solution (PBS), Hank's Balanced Salt Solution (HBSS), and trypsin (0.25%) supplemented with 0.53 mmol/L EDTA were all obtained from Wisent Bioproducts (St. Bruno, QC, Canada). Opti-MEM Reduced Serum Medium was acquired from Invitrogen (Burlington, ON, Canada). Salmon sperm DNA (SSD) and polyethyleneimine (PEI) were sourced from Sigma-Aldrich (Oakville, ON, Canada). Coelenterazine 400A (Deep Blue C) was provide by GoldBio (Gold Biotechnology, St-Louis, MO, USA). White opaque 96-well plates were purchased from BD Falcon (Corning, NY, USA). 96-well plates with gold-plated interdigitated finger electrodes for Electric Cell-substrate Impedance Sensing (ECIS) were purchased from Applied Biophysics (Troy, NY, USA).

2.2. *Pepducin synthesis*

NTSR1-derived pepducins were synthesized using standard C→N solid-phase peptide synthesis, with 12 mL polypropylene cartridges with 20 μm PE frit (Applied Separations, Allentown, PA, USA). 250 μmol of TentaGel S RAM resin (0.24 mmol/g) were deprotected with a mixture of piperidine:DMF (1:1) for 2 × 10 min. The fmoc-protected amino acids (3 eq.) were coupled using HATU (3 eq.) and DIEA (6 eq.) in DMF (10 mL) for at least 2 h. The reactant and solvent were then filtered, and the resin was washed with 10 mL DMF (2 × 5 min under agitation) and three alternating cycles of washing with 2-propanol (7 mL) or DCM (7 mL). Deprotection cycles were carried out with a mixture of piperidine: DMF (1:1) for 2 × 10 min. After deprotection, the solvent was removed by filtration, the resin was washed with DMF, 2-propanol, and DCM (as described above), and the Fmoc-protected amino acid was then coupled using HATU/DIEA in DMF. Coupling of palmitate (3 eq.) was done in dry *N*-methyl-2-pyrrolidone (NMP) with HATU (3 eq.) and DIEA (6 eq.).

Peptides and pepducins were cleaved from the resin using 92.5% TFA, 2.5% TIPS, 2.5% H2O, and 2.5% EDT for at least 2 h to provide the crude mixture of the desired peptide. The resin suspension was filtered through cotton wool and the peptide precipitated in 50 mL of tert-butyl methyl ether at 0 °C. The suspension was centrifuged for 20 min at 1500 rpm, and the pellet was resuspended in a mixture of water:acetonitrile (2:1) and lyophilized before purification.

Purification was done on a Waters Mass-triggered preparative HPLC system (Sample Manager 2767, Binary Gradient Module 2545, with two 515 HPLC pumps, a System Fluidics Organizer, and a 2998 Photodiode Array Detector) combined to a SQ Detector 2 and equipped with an X Select CSH Prep C18 5 mm OBD 19 mm × 250 mm column using a 25%−40% gradient of acetonitrile with 0.1% formic acid for 15 min. The fractions were analyzed by UPLC/MS (Water H Class Acquity UPLC, mounted with Acquity UPLC BEH C_{18} column, 1.7 μm, 2.1 mm × 50 mm, and paired to a SQ Detector 2) using a gradient of 5%−95% acetonitrile with 0.1% formic acid for 2 min. Fractions with a purity of 95% or greater were then lyophilized and stored at −20 °C until use. HRMS was performed on a Bruker MaXis 3G high-resolution Q-ToF. Purified product yielded a white powder after being freeze-dried. Stock solutions in 100% DMSO were prepared for biological assays at 10-mmol/L concentrations.

2.3. Plasmids and constructs

The cDNAs encoding hNTSR1 and the $G\beta_1$ subunit were purchased from the Bloomsburg University cDNA Resource Center (Bloomsburg, PA, USA). Those encoding $G\alpha_q$-RlucII[51], $G\alpha_{i1}$-RlucII[52], $G\alpha_{oA}$-RlucII[53], $G\alpha_{13}$-RlucII[54], GFP10-$G\gamma_1$[55,56], RlucII-β-arrestin-1[57] or -2[58], and rGFP-CAAX[59] were kindly provided by Dr. Michel Bouvier (Université de Montréal). The plasmids encoding NTSR1-GFP10[60] and APJ-GFP10[61] were previously constructed by our team using an InFusion advantage PCR cloning kit (Clontech Laboratories, Mountain View, CA, USA). To generate the NTSR1-RlucII and APJ-RlucII constructs for this study, the complete coding sequences of hNTSR1 and hAPJ receptors were amplified by PCR without their stop codons, inserted in frame into a pIRES(puroR)-RlucII-StrepTagII vector following BamHI digestion, and fused to RlucII by a 7 amino acid GSGSAGT linker using the InFusion advantage PCR cloning kit according to the manufacturer's recommendations. Finally, a 3xHA-hNTSR1 pcDNA3.1 construct was purchased from the Bloomsburg University cDNA Resource Center (Bloomsburg, PA, USA) and provided to GenScript (Piscataway, NJ, USA) as the template for the construction of the 27 NTSR1 ICL mutant cDNAs (ICL Mutants 1−27). The specific mutations introduced are provided in Supporting Information Table S7. Constructs were verified by DNA sequencing before use. Engineered recombinant NTSR1−3 and NTS-22 were constructed using standard cloning procedures and polymerase chain reaction. The receptor modifications are presented in Supporting Information Fig. S2 and Table S6, as described elsewhere[62,63].

2.4. Cellular assays

2.4.1. Cell culture and transfections

Multiple cell lines were used to characterize the *in vitro* behavior of our pepducin series. Chinese hamster ovary cells (CHO-K1, CCL-61 from ATCC, Manassas, VA, USA) were cultured in DMEM-F12 medium supplemented with 20 mmol/L HEPES, 10% FBS, and penicillin (100 U/mL)-streptomycin (100 mg/mL). CHO-K1 cells stably expressing hNTSR1 (CHO-hNTSR1, ES-690-C), purchased from PerkinElmer (Montreal, QC, Canada), were cultured in the same conditions but further supplemented with 0.4 mg/mL of geneticin (G418). Human embryonic kidney 293 (HEK293) cells were cultured in DMEM supplemented with 20 mmol/L HEPES, 10% FBS, and penicillin (100 U/mL)-streptomycin (100 mg/mL). All cell lines were maintained in a humidified atmosphere at 37 °C and 5% CO_2 and were used between passages 5 and 25.

For transient expression of recombinant proteins, 100-mm cell culture dishes were seeded with 2×10^6 cells. Cells were transfected 24 h later with 12 mg cDNA; if the amount of cDNA required for the assay did not reach this total, transfection mixes were completed with SSD. Transfection complexes were formed by incubating plasmids for 25 min in Opti-MEM serum-free media with the transfection reagent polyethyleneimine (PEI) at a 3:1 PEI:cDNA ratio[64], then gently deposited onto cells.

2.4.2. Bioluminescence resonance energy transfer (BRET) assays

2.4.2.1. G protein dissociation and βarr recruitment. To monitor G protein dissociation, CHO-K1 cells were transfected with either $G\alpha_q$-RlucII, $G\alpha_{i1}$-RlucII, $G\alpha_{oA}$-RlucII, or $G\alpha_{13}$-RlucII, as well as GFP10-$G\gamma_1$, $G\beta_1$, and hNTSR1. To monitor βarr recruitment, CHO-K1 cells were transfected with RlucII-β-arrestin 1 or RlucII-β-arrestin 2 and NTSR1-GFP10. At 24 h post-transfection, the cells were detached with trypsin (0.25%) containing 0.53 mmol/L EDTA and plated (50,000 cells/well) in white opaque 96-well plates. At 48 h post-transfection, the cells were washed once with HBSS, and 90 μL of HBSS containing 20 mmol/L HEPES was added (or 80 μL for the allosteric modulator assays). Cells were equilibrated for 1 h at 37 °C. In the agonist assays, cells were stimulated for 10 min with increasing concentrations of NT(8-13) (10^{-6} to 10^{-12} mol/L) or NTSR1-derived pepducins (10^{-4} to 10^{-8} mol/L), followed by coelenterazine 400A (5 μmol/L). In the allosteric modulator assays, cells were first stimulated with fixed concentrations of the pepducins (0, 1, 10, 32, 100 μmol/L) for 10 min, followed by increasing concentrations of NT or NT(8-13) (10^{-6} to 10^{-12} mol/L) and coelenterazine 400A (5 μmol/L). Plates were read multiple times over a 20-min period, using a Mithras^2 LB 943 plate reader (Berthold Technologies, Oak Ridge, TN, USA) with a filter set selected for BRET^2 measurement (λem_{RlucII} 410 ± 80 nm; λem_{GFP10} 515 ± 40 nm) set to a 1-s integration time. The BRET^2 ratio was set at 515:410 nm (GFP10 emission:RlucII-coelenterazine 400A emission).

2.4.2.2. Receptor endocytosis. To monitor NTSR1 receptor endocytosis, CHO-K1 cells were transfected with NTSR1-RlucII and rGFP-CAAX using the transfection reagent PEI, then transferred into 96-well opaque white plates 24 h later, as described above. At 48 h post-transfection, cells were washed with HBSS, received 90 μL of HBSS containing 20 mmol/L HEPES (or 80 μL for the allosteric modulator assays), and were equilibrated for 1 h at 37 °C. In the agonist assays, cells were first stimulated with coelenterazine 400A (5 μmol/L), and BRET^2 luminescence was recorded on a Mithras^2 LB 943 plate reader (Berthold Technologies, Oak Ridge, TN, USA) for 5 min at 20-s intervals, to acquire a baseline pre-pepducin stimulation. Cells were then stimulated with vehicle (HBSS, 1% DMSO), NT(8-13) (1 μmol/L), or NTSR1-derived pepducins (50 μmol/L), and BRET^2 was recorded for a further 30 min at 20-s intervals (0.5-s integration time) at 37 °C. In the allosteric modulator assays, cells were first stimulated with vehicle (HBSS, 1% DMSO) or with NTSR1-derived pepducins (50 or 100 μmol/L) and incubated at 37 °C for 10 min, before receiving 5 μmol/L of coelenterazine 400A. As above, BRET^2 was recorded for 5 min at 20-s intervals before stimulation with HBSS or NT(8-13) (1 μmol/L), then monitored for a further 30 min. BRET^2 ratios for each condition were normalized to reflect a BRET^2 change factor: BRET^2 ratios at each time-point were compared to (divided by) baseline BRET^2 ratios. These normalized responses were then compared to (subtracted from) those of the vehicle condition (or vehicle + HBSS condition).

2.4.2.3. Receptor homo- and heteromerization. To monitor NTSR1-NTSR1 homomeric or NTSR1-APJ heteromeric interactions, BRET^2 titration experiments were performed using the biosensor couples hNTSR1-RlucII and hNTSR1-GFP10; hNTSR1-RlucII and hAPJ-GFP10; or hAPJ-RlucII and hNTSR1-GFP10. CHO-K1 cells (NTSR1-NTSR1 homomer experiments) or HEK293 cells (NTSR1-APJ heteromer experiments) were seeded (300,000 cells/well) onto 6-well cell culture dishes and transfected 24 h later with transfection complexes. Each condition received a total of 2.1 μg cDNA, corresponding to fixed amounts (50, 100 ng) of 7TMR-RlucII and increasing amounts (0−2 μg) of 7TMR-GFP10. Transfection mixes were completed with SSD. At 24 h post-transfection, cells were detached with trypsin (0.25%)

supplemented with 0.53 mmol/L EDTA and plated (100,000 cells/well) into white opaque 96-well plates. At 48 h post-transfection, cells were washed once with HBSS and received 90 μL of HBSS supplemented with 20 mmol/L HEPES. Cells were then equilibrated for 1 h at 37 °C, after which they were stimulated with buffer, with NT(8-13) or Apelin-13 (1 μmol/L), or with NTSR1-derived pepducins (50 or 100 μmol/L) for 10 min, followed by coelenterazine 400A (5 μmol/L). Plates were read multiple times over a 20-min period, using a Mithras^2 LB 943 plate reader (Berthold Technologies, Oak Ridge, TN, USA) with a filter set selected for BRET^2 measurement (λem_{RlucII} 410 ± 80 nm; λem_{GFP10} 515 ± 40 nm). The BRET^2 ratio was determined as GFP10em/RlucIIem. Baseline BRET^2 ratios (condition with no transfected 7TMR-GFP10) were subtracted from each condition's BRET^2 ratios to obtain ΔBRET^2.

2.5. *Pepducin GPCRome*

To probe the specificity of the NTSR1-derived pepducins, a stock solution of PP-001 was sent for testing to the NIMH Psychoactive Drug Screening Program (PDSP) directed by Dr. Bryan Roth (UNC School of Medicine, North Carolina, USA), an open-source resource for interrogating the druggable GPCRome[65]. The PRESTO-Tango assays were performed as has been previously described. Briefly, HTLA cells (HEK293 cells stably expressing a tTA-dependent luciferase reporter and a βarr2-TEV fusion protein) were plated into 384 well plates and incubated overnight, before transfection with cDNA coding for 318 distinct 7TMR-Tango constructs, using a calcium phosphate precipitation protocol. On the day of testing, cells were serum-starved for 4 h, then stimulated with 10 μmol/L PP-001 prepared in Tango assay buffer. As positive and negative controls, respectively, D2R-Tango-expressing cells were stimulated with quinpirole and non-transfected cells were stimulated with PP-001. Plates were incubated overnight. Media was removed and BrightGlo reagent (Promega) solution (20 μL) was added subsequently. Plates were incubated for 20 min in the dark before luminescence reading. Four independent experiments were performed in duplicate. Data are reported (Supporting Information Table S1) in decreasing order of fold-change.

2.6. *Radioligand binding*

To determine the pepducins' ability to affect orthosteric NT binding at the NTSR1 receptor, competitive radioligand binding assays were performed. CHO-hNTSR1 cells were cultured as described above; once 80% confluency was reached, cells were washed with PBS and frozen at −80 °C. Frozen cells were thawed, scraped from the dish with 10 mmol/L Tris buffer with 1 mmol/L EDTA (pH 7.5) and centrifuged at 15,000×*g* for 5 min at 4 °C. The pellet was resuspended in binding buffer (50 mmol/L Tris-HCl [pH 7.5], 0.2% BSA). 15 μg of cell membranes expressing the hNTSR1 receptor were incubated with 45 pmol/L ^{125}I-[Tyr3]-NT (2200 Ci/mmol, purchased from PerkinElmer, Billerica, MA, USA) in the presence of increasing concentrations of NT(8-13) (10^{-12} to 10^{-6} mol/L), PP-001, NP-001, PP-SCR-001, [Ala^2]PP-001, or [Ala^{13}]PP-001 (10^{-8} to 10^{-4} mol/L) for 60 min at room temperature.

In the binding experiments performed with HA-hNTSR1 and the ICL mutants (Mutants 1−27, whose sequences are shown in Table S7), HEK293 cells were transfected with 6 μg of cDNA, completed to 12 μg with SSD. At 24 h post-transfection, cells were washed with PBS and frozen at −80 °C. Cells were scraped, centrifuged, and resuspended in 1 mL of binding buffer without BSA (50 mmol/L Tris−HCl [pH 7.5]). Cell membranes were quantified using the Pierce BCA Protein Assay Kit (Thermo Fisher Scientific, Montreal, QC, Canada) according to the manufacturer's instructions. Cell membrane suspensions were re-prepared in 6 μg/well of binding buffer (50 mmol/L Tris−HCl [pH 7.5], 0.2% BSA). ICL mutants were subdivided into 3 groups relative to their cell surface expression data: Group 1 (full cell surface expression), including Mutants 3, 6, 7, 9, 10, 11, 12, 13, 15, 21, 22, 23, 24, 25, 26, and 27; Group 2 (partial cell surface expression), including Mutants 2, 5, 8, 14, 16, 17, and 20; and Group 3 (poor cell surface expression), including Mutants 1, 4, 18, and 19. Cell membranes were incubated with ^{125}I-[Tyr^3]-NT (2200 Ci/mmol) in binding buffer in the presence of increasing concentrations of NT(8-13) (10^{-12} to 10^{-6} mol/L) or PP-001 (10^{-6} to 10^{-4} mol/L) for 60 min at room temperature; Group 1 cell membranes were incubated with 90 pmol/L ^{125}I-[Tyr^3]-NT, Group 2 cell membranes with 180 pmol/L ^{125}I-[Tyr^3]-NT, and Group 3 cell membranes with 300 pmol/L ^{125}I-[Tyr^3]-NT.

After incubation, the binding reaction mixtures were transferred to PEI-coated 96-well filter plates (glass fiber filters GF/B, Millipore, Billerica, MA, USA). Reaction was terminated by filtration, and plates were washed three times with 200 μL of ice-cold binding buffer. Glass filters were then counted using a γ-counter (2470 Wizard2, PerkinElmer, Mississauga, ON, Canada). Nonspecific binding was measured in the presence of 10^{-5} mol/L unlabeled NT(8-13) and represented less than 5% of total binding. Data were normalized according to NT(8-13) to control for unwanted sources of variation.

2.7. *Electric cell-substrate impedance sensing (ECIS)*

To monitor whole-cell integrative responses to pepducin treatment, CHO-hNTSR1 cells were seeded (35,000 cells/well, 300 μL/well) onto cysteine-stabilized, Poly-L-Lysine-coated 96-well plates with interdigitated finger gold-plated electrodes (96W20idf) purchased from Applied Biophysics (Troy, NY, USA) and used as recommended by the manufacturer. Cells were cultured in serum-containing media for 24 h, then serum-starved for 16−18 h prior to the experiment. On the day of the experiment, the cells were washed with PBS and received 90 μL of L-15 modification medium. The biophysical parameters of the cell monolayer (*i.e.*, electrical resistance to a 4000-Hz single frequency AC current) were recorded with an ECIS Zθ linked to a 96-well array station (Applied Biophysics, Troy, NY, USA) for a minimum period of 60 min prior to compound stimulation, to acquire a stable baseline. Cells were treated with L-15 media or 10 μmol/L of PP-001, PP-SCR-001, or the PP-001 alanine scan series ([Ala^2]PP-001, [Ala^3]PP-001, [Ala^4]PP-001, … [Ala^{14}]PP-001). The dynamic mass redistribution (DMR) dynamics were then recorded for a further 60 min post-compound stimulation. The electrical resistivity traces shown represent the averaged normalized response, calculated as the resistance of the cell monolayer (ohms) divided by the average baseline resistance (ohms) prior to compound stimulation.

2.8. *Cell surface expression of NTSR1 ICL mutants*

To determine the cell surface expression of the 27 NTSR1 ICL mutants (whose sequences are shown in Table S7), ELISA was conducted. HEK293 cells were seeded (100,000 cells/well) into

24-well plates coated with poly-L-Lysine and transfected with cDNA (415 ng/well) coding for WT HA-hNTSR1 receptor or HA-hNTSR1 ICL mutants (Mutants 1−27) using PEI (3:1 PEI:cDNA). Then, 48 h post-transfection, cells were fixed with 3.7% (*v*/*v*) formaldehyde in Tris-buffered saline (TBS, 20 mmol/L Tris−HCl [pH 7.5], and 150 mmol/L NaCl) for 5 min at room temperature. Cells were washed three times with TBS and incubated for 45 min in TBS supplemented with 3% (*m*/*v*) fat-free dry milk to block nonspecific binding sites. A mouse monoclonal anti-HA antibody coupled to HRP (Roche) was added at a 1:1000 dilution in TBS 3% fat-free milk and incubated for 2 h at room temperature on a nutating mixer. Following incubation, cells were washed three times with TBS before receiving 250 µL of 3,3′5,5′-Tetramethylbenzidine (TMB, Sigma−Aldrich, Oakville, ON, Canada). Plates were incubated for 15 min at room temperature, or until the colorimetric reaction (colorless to blue) was complete for the positive control (WT). The reaction was stopped by adding 250 µL of HCl 2N. At that point, 200 µL of the yellow reaction product was transferred to 96-well plates, and the absorbance was read at 450 nm on a Mithras^2 LB 943 plate reader (Berthold Technologies, Oak Ridge, TN, USA). Cells transfected with the empty pcDNA3.1+ vector (mock) were used to determine background.

2.9. Expression and protein purification of NTSR1−3 and NTSR1−22

NTSR1−3 and NTSR1−22 were expressed in *Sf9* insect cells using Bac-To-Bac Bacculovirus Expression System (Thermo Fisher Scientific). Membrane form cells expressing NTSR1−3 or NTSR1−22 were prepared using three rounds of washing and ultracentrifugation at 250,000×*g*, first in the presence of lysis buffer containing 10 mmol/L HEPES (pH 7.5), 20 mmol/L KCl, and 10 mmol/L $MgCl_2$, and twice with a washing buffer containing 10 mmol/L HEPES (pH 7.5), 1 mol/L NaCl, 20 mmol/L KCl, and 10 mmol/L $MgCl_2$. The purified membrane was then resuspended in the lysis buffer supplemented with 20% (*v*/*v*) glycerol. 1 mmol/L benzamidine and 5 µg/mL leupeptin were added for the first two steps. The membranes were then incubated for 1 h at 4 °C with protease inhibitors, 1 mg/mL iodoacetamide, and 15 µmol/L NT(8-13). The receptor was then solubilized in 50 mmol/L HEPES (pH 7.5), 800 mmol/L NaCl, 0.5% (*w*/*v*) *n*-dodecyl-β-D-maltopyranoside (DDM, Anatrace, Maumee, OH, USA), and 0.1% (*w*/*v*) cholesteryl hemisuccinate (CHS, Sigma−Aldrich) in the presence of protease inhibitors. The supernatant was isolated by ultracentrifugation for 1 h at 350,000×*g* and then incubated with TALON resin (TALON Superflow beads, Cytiva, Wilmington, DE, USA) overnight at 4 °C. The TALON resin was washed with 20 column volumes of wash buffer 1 containing 50 mmol/L HEPES (pH 7.5), 150 mmol/L NaCl, 20 mmol/L $MgCl_2$, 20 mmol/L imidazole, 8 mmol/L ATP, 10% (*v*/*v*) glycerol, 0.1% (*w*/*v*) DDM, 0.02% (*w*/*v*) CHS, and 15 µmol/L NT(8-13), followed by 10 column volumes of wash buffer 2 containing 50 mmol/L HEPES (pH 7.5), 150 mmol/L NaCl, 30 mmol/L imidazole, 10% (*v*/*v*) glycerol, 0.05% (*w*/*v*) DDM, 0.01% (*w*/*v*) CHS, and 15 µmol/L NT(8-13). The receptor was eluted using 2.5 column volumes of elution buffer containing 50 mmol/L HEPES (pH 7.5), 150 mmol/L NaCl, 250 mmol/L imidazole, 10% (*v*/*v*) glycerol, 0.01% (*w*/*v*) DDM, 0.002% (*w*/*v*) CHS, and 15 µmol/L NT(8-13). Finally, an Amicon Ultra 0.5 mL 100K (Millipore, Oakville, ON, Canada) was used to concentrate NTSR1−3 and NTSR1−22 at a concentration of 5 mg/mL.

2.10. Thermodenaturation assays

7-Diethylamino-3-(4-maleimidophenyl)-4-methylcoumarin (CPM) was obtained from Thermo Fisher Scientific (Mississauga, ON, Canada) and resuspended in DMSO at a concentration of 500 µmol/L. The assay used 30 or 40 µg of purified NTSR1−3 or NTSR1−22, respectively. The protein was added to a reaction buffer containing 50 mmol/L HEPES (pH 7.5), 150 mmol/L NaCl, 0.05% (*w*/*v*) DDM, 0.001% (*w*/*v*) CHS, and 10 µmol/L CPM. The mixture was incubated in the presence of 100 µmol/L of indicated ligand or vehicle for 20 min at room temperature. Unfolding of NTSR1 was induced using a Rotor-Gene Q (Qiagen. Bay St., ON, Canada) thermocycler by slowly increasing the sample temperature (+0.5 °C per step from 30 to 95 °C), resulting in an emission of a fluorescence signal detected in the blue channel (excitation 365 nm/emission 460 nm) from CPM chemical reaction to newly exposed receptor cysteines[66]. The melting temperature was determined by the maximum of the first derivative of the normalized thermodenaturation curve using GraphPad Prism 10.

2.11. Molecular modeling

2.11.1. Receptor model

The NT(8-13)−bound rat neurotensin receptor 1 (NTSR1) crystal structure (PDB 4GRV) was used as the starting template[67]. Missing side chains were rebuilt in MOE v2024.0601, hydrogens were added, and protonation states at pH 7.4 were assigned with Protonate3D (Chemical Computing Group ULC. Molecular Operating Environment (MOE), 2024.06; CCG: Montreal, QC, Canada, 2024). The receptor−ligand complex (NTSR1 with NT(8-13) retained in the orthosteric site) was embedded into a symmetric 1-palmitoyl-2-oleoylphosphatidylcholine (POPC) bilayer using CHARMM-GUI Membrane Builder, solvated with TIP3P water and 150 mmol/L NaCl[68]. All simulations were performed in GROMACS v2023.2[69]. The CHARMM36m protein and lipid force field parameters were used with PME electrostatics, a 1.2 nm real-space cutoff (force-switch 1.0−1.2 nm), LINCS constraints on bonds involving hydrogens, and a 1−2 fs time step[70]. Following steepest-descent energy minimization, the system was equilibrated with standard CHARMM-GUI restraints: (i) six NVT/NPT stages totaling ∼2 ns with positional restraints on protein heavy atoms and lipid headgroups (force constants decreased from 4000 → 0 kJ/mol·nm^2), then (ii) unrestrained NPT production for 100 ns at 303.15 K and 1 bar using a velocity-rescale thermostat (τT = 1.0 ps, semi-isotropic coupling) and C-rescale barostat (τP = 5.0 ps, compressibility 4.5×10^{-5} bar^{-1})[70−77]. The final equilibrated snapshot was extracted as the receptor for docking (NT retained).

2.11.2. Pepducin (PP-001) model

PP-001 is a 10-residue lipidated peptide with an N-terminal palmitoyl group and an amide C-terminus as in functional experiments. An initial 3D model was generated with the RoseTTAFold2 web server, then checked in MOE for stereochemistry and capped/charged to match experimental conditions[78,79]. The palmitoyl group was attached at the N-terminus; standard protonation states were used at pH 7.4. Partial charges and parameters for the peptide were assigned by MOE's default force-field typing for docking.

2.11.3. Docking protocol

Docking was performed in MOE v2024.0601 using the "Dock" module with the General docking scenario and two-stage workflow; Placement: Triangle Matcher; Rescoring 1: London dG and 30 top-scoring poses per input conformer. Refinement: Induced-Fit (Forcefield) with local receptor flexibility enabled in the selected H8/ICL pocket (side chains free within the pocket; non-selected atoms tethered with a 10 kcal mol^{-1} $Å^{-2}$ force constant; reaction-field electrostatics, GB/VI final energy). Rescoring 2: GBVI/WSA dG and final keep: 10 poses[80]. No hard distance restraints were applied; the site definition confined sampling to the intracellular groove while allowing the pepducin and pocket side chains to reorganize. Because PP-001 acts at the cytoplasmic face, the docking site was defined on the intracellular side of NTSR1. A receptor surface surrounding ICL1, ICL2, ICL3, and H8 was selected in MOE as the docking region. The orthosteric peptide NT(8-13) was kept in place throughout to enforce a non-competitive topology during search and refinement.

2.12. Blood pressure

The animal experimental procedures approved by the Ethical and Animal Care Committee of the Université de Sherbrooke (protocol 035-18B) were conducted in accordance with the policies and directives of the Canadian Council on Animal Care, and followed the ARRIVE Guidelines. Adult male Sprague−Dawley rats (250−300 g) were purchased from Charles River Laboratories (Saint-Constant, QC, Canada) and kept on a 12 h light/12 h dark cycle with ad libitum access to food and water.

To monitor pepducin-induced changes in rat arterial blood pressure, male Sprague−Dawley rats were anesthetized with a mixture of ketamine and xylazine (87:13 mg/kg, i.m.) and placed in a supine position on a heated thermostatic pad. A PE50 catheter with heparinized saline was inserted into the rat's right carotid artery and connected to a Micro-Med transducer (model TDX-300) linked to a blood pressure Micro-Med analyzer (model BPA-100c). Another PE10 catheter with heparinized saline was inserted into the left jugular vein for intravenous injection of compounds. Mean, systolic, and diastolic blood pressure, as well as heart rate, were recorded at 1-s or 5-s intervals for the duration of the test. Once basal blood pressure was stable, rats received 10-s bolus injections (1 mL/kg) of saline, vehicle (saline, 5% DMSO), or 55 nmol/kg dose solutions of NT(813), PP-001, NP-001, PP-SCR-001, [Ala^2]PP-001, and [Ala^{13}]PP-001. In the SR48692 + PP-001 group, rats were injected with the non-peptide antagonist SR48692 (1 mg/kg) 10 min prior to PP-001 administration. DMABP was determined relative to baseline. The minimum blood pressure relative to baseline (maximum DMABP) for each individual animal was determined, and values were pooled.

2.13. Statistical analysis

All data obtained for this study were plotted onto graphs using GraphPad Prism 10 software (RRID:SCR_002798) and represent the mean ± standard error of mean (SEM) of multiple independent experiments. Specific *n* values are provided in the figure legends. Sigmoidal concentration-response curves were plotted using the "log(agonist) *vs*. response (three-parameters)" regression or, in the case of the binding experiments, using the non-linear regression "One-site-Fit Log(IC_{50})". pEC_{50} (or pIC_{50}) and E_{max} values were compared using one-way ANOVA tests with Dunnett's correction for multiple comparisons. Titration curves were plotted using the "one-site-specific binding" regression for binding saturation experiments. Similarly, $BRET_{50}$ and $BRET_{max}$ values were compared using one-way ANOVA with Dunnett's correction. Otherwise, the details for data normalization, statistical analysis, and *P* values are provided in the figure legends.

3. Results

3.1. PP-001 preferentially promotes G protein activation over βarr recruitment

We recently designed and synthesized a pepducin series derived from the first intracellular loop (ICL1) of hNTSR1[42]. This series included a full-length ICL1 pepducin (NTSR1-ICL1-PP-001), a non-palmitoylated control (NTSR1-ICL1-NP-001), and a pepducin with a scrambled peptide sequence (NTSR1-ICL1-PP-SCR-001), which will be referred to throughout this paper by the abbreviations PP-001, NP-001, and PP-SCR-001, respectively. Their sequences, along with those of all peptides and lipopeptides tested throughout this study are provided in Table 1. Importantly, pepducin PP-001 has been shown to be effective in reversing nociceptive behaviors in rats, even in chronic neuropathic and inflammatory pain paradigms[42]. Here, we have thoroughly investigated the signaling profile of PP-001 by evaluating the activation of $G\alpha_q$, $G\alpha_{i1}$, $G\alpha_{oA}$, $G\alpha_{13}$, βarr1, and βarr2 signaling pathways in NTSR1-expressing cells in response to a range of pepducin concentrations. (Please note that the β-arrestins 1 and 2 (here, βarr1 and βarr2) can be referred to by the alternative names arrestin-2 and arrestin-3).

To do so, we relied on bioluminescence resonance energy transfer ($BRET^2$)-based cellular assays designed to monitor G protein dissociation and βarr recruitment, the principles of which are illustrated inFig. 1a and b, respectively (Note that these schemas depict the classical mode of 7TMR activation by an extracellular, orthosteric ligand, whereas pepducins are thought to modulate their target receptor by acting on an intracellular allosteric site[14]). These assays, which monitor the interaction between donor-tagged (RlucII) and acceptor-tagged (GFP10) proteins, were performed 30 min after stimulation with pepducins in transiently transfected CHO-hNTSR1 cells. The $BRET^2$ ratios obtained were compared to NT's C-terminal hexapeptide, NT(8-13). This hexapeptide represents the minimal biologically active fragment of NT[81] and has been shown to exhibit a signaling signature identical to that of NT in CHO-hNTSR1 cells[60]. NT(8-13) is therefore used as the reference compound in this study.

As shown in Fig. 1c and d, our results are consistent with a biased signaling paradigm. Indeed, stimulation with PP-001 led to a marked increase in signaling pathway activation in the G protein dissociation assays. Maximum values of 41 ± 9% ($G\alpha_q$), 43 ± 13% ($G\alpha_{i1}$), 67 ± 11% ($G\alpha_{oA}$), and 68 ± 7% ($G\alpha_{13}$) pathway activation were obtained at 100 μmol/L PP-001. However, no recruitment of βarr1 and βarr2 at NTSR1 was observed at the same concentration. Importantly, neither NP-001 nor PP-SCR-001 induced any change in $BRET^2$, and thus do not appear to affect G protein signaling or βarr recruitment. Given that none of the G protein-related concentration−response curves could be fitted to a complete sigmoidal regression, including a second maximal plateau, we were unable to determine reliable potencies (EC_{50}) for PP-001. Without these reliable potencies, we were also unable to do traditional bias quantifications using approaches based on determining intrinsic relative activity (RA_i) values[82,83] or comparing transduction coefficients (t/K_a)[84] derived from the

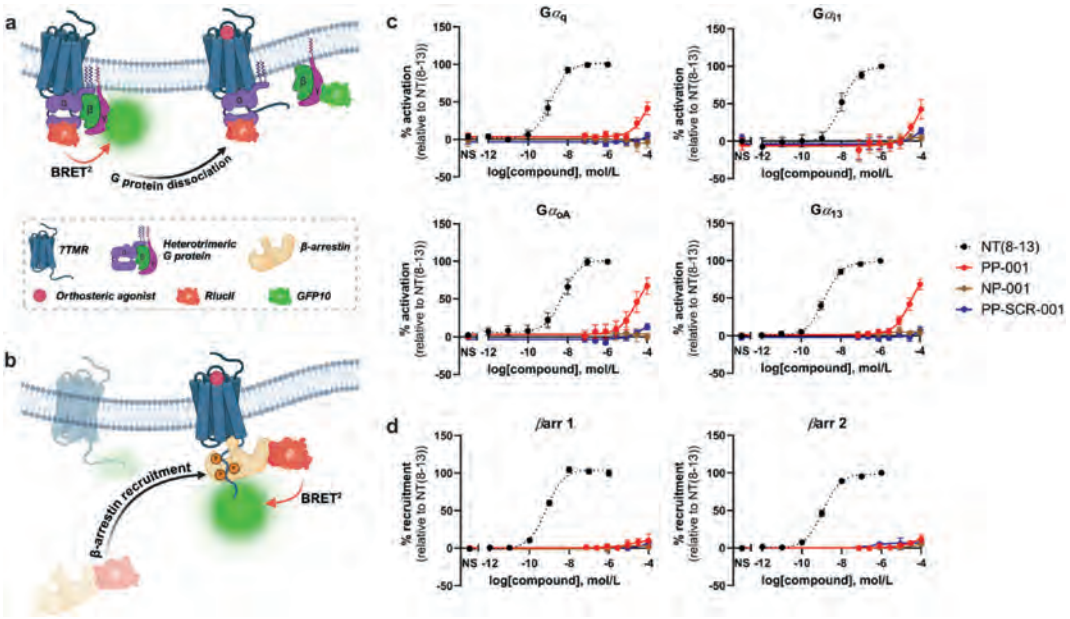

Figure 1 PP-001 activates G protein signaling pathways but does not recruit s to NTSR1. (a) Principle of the BRET^2 G protein dissociation assay. Agonist-induced G protein activation leads to a loss of BRET^2 signal, as donor-tagged (RlucII) Gα proteins and acceptor-tagged (GFP10) Gγ proteins dissociate. (b) Principle of the BRET^2 recruitment assay. The BRET^2 signal increases as donor-tagged (RlucII) cytosolic s are recruited to the acceptor-tagged (GFP10) receptor, after agonist binding. (c) Gα protein dissociation in CHO-K1 cells transiently expressing the NTSR1 receptor, monitored by BRET^2, in response to increasing concentrations of NT(8-13), PP-001, NP-001, or PP-SCR-001. (d) Recruitment in CHO-K1 cells, monitored by BRET^2, in response to increasing concentrations of NT(8-13), PP-001, NP-001, or PP-SCR-001. Data represent the mean ± SEM of at least three independent experiments, tested in triplicate. Luminescence was measured 30 min after pepducin stimulation. BRET^2 ratios were normalized to NT(8-13): data from vehicle-treated cells were set as 0% activation (or recruitment) and data from NT(8-13) (1 μmol/L)-treated cells were set to 100% activation (or recruitment). Schemas were created with Biorender.com. NS: non-stimulated (treated with vehicle only).

Black and Leff operational model[85]. However, the complete lack of PP-001-mediated βarr recruitment at 100 μmol/L strongly suggests that PP-001 behaves as a G protein-biased allosteric agonist. In addition, PP-001 did not induce βarr2 recruitment across a panel of 318 distinct 7TMRs, as determined using the PRESTO-Tango assay[65], supporting its selective activity at NTSR1 (Table S1).

3.2. PP-001 inhibits NT orthosteric binding and NT-induced βarr recruitment

PP-001 appears to act as a biased allosteric agonist of NTSR1, preferentially activating G protein signaling pathways over βarr recruitment. However, it is now recognized that allosteric ligands can assume multiple identities, leading to classifications such as "ago-PAM" or "ago-NAM" (*i.e.*, compounds that act as allosteric agonists in one signaling pathway, but as PAMs or NAMs in another)[86]. As a result, we sought to determine whether treatment with PP-001 also affects NT binding at the orthosteric site or the activation of NT-promoted signaling pathways.

First, we tested PP-001 in a competitive radioligand binding assay. For this purpose, CHO-hNTSR1 cell membrane preparations were incubated with radiolabeled NT ([^{125}I]-NT) in the presence of increasing concentrations of unlabeled ligands. As shown in Fig. 2a, the pepducin PP-001 inhibited radiolabeled NT binding in a concentration-dependent manner, with an IC_{50} of 5.5 ± 0.8 μmol/L and complete inhibition at 100 μmol/L. As expected, NT(8-13) displaced radiolabeled NT with an IC_{50} of 1.0 ± 0.1 nmol/L. Importantly, the peptide sequence of PP-001 alone (NP-001) had no effect on NT binding, suggesting that this "displacement" induced by PP-001 is not due to direct competition with NT at the orthosteric site, but results from the insertion of PP-001 into the membrane and its allosteric action. PP-SCR-001 was largely inactive, but slighly reduced NT binding at 100 μmol/L.

Second, we performed BRET^2 experiments to monitor G protein dissociation and βarr recruitment in an allosteric modulator-type assay, in which full concentration−response curves of NT were generated in cells pre-treated with fixed, but increasing concentrations of pepducins. As shown in Fig. 2b and c, pre-treating cells with PP-001 led to divergent effects in G protein versus βarr assays. In G protein dissociation assays, PP-001 increased the basal levels of pathway activation in a concentration-dependent manner, consistent with its previously determined allosteric agonist action. Treatment with PP-001 did not change NT's E_{max} in a statistically significant manner (Supporting Information Table S2). Additionally, although we observed a slight shift in NT's EC_{50} values in each G protein pathway, this was accompanied by a corresponding increase in SEM. Therefore, we cannot conclude that NT's potency was affected by PP-001 pre-treatment. If PP-001 inhibited NT-mediated signaling, as might be expected from the radioligand binding experiments, this result was effectively masked by its agonist action on G protein signaling.

In the βarr assays, however, there was a clear inhibitory effect on NT-mediated recruitment. A concentration-dependent decrease

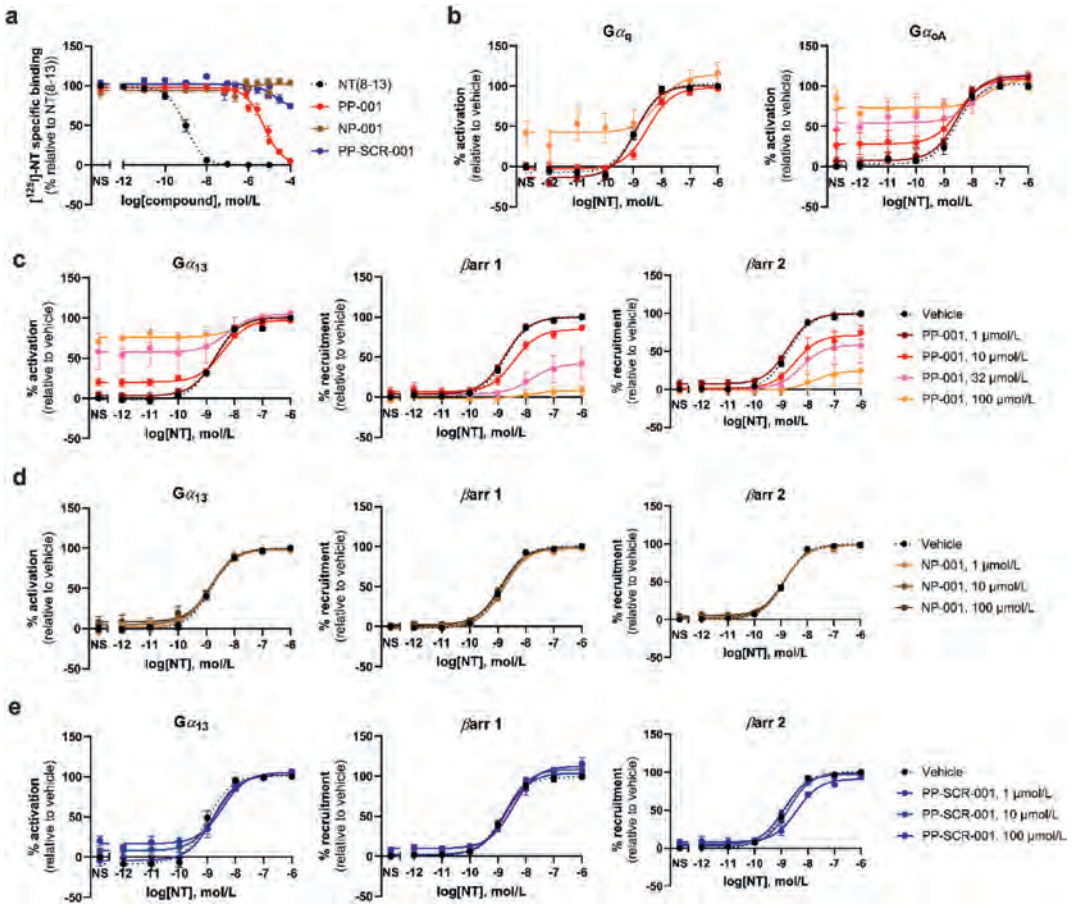

Figure 2 PP-001 allosterically inhibits NT binding and NT-promoted recruitment, but not NT-promoted G protein activation. (a) Displacement of ^{125}I-radiolabeled NT following incubation of CHO-hNTSR1 membranes with increasing concentrations of unlabeled NT(8-13), PP-001, NP-001, or PP-SCR-001 in a competitive radioligand binding assay. (b, c) NT-induced G protein dissociation and recruitment in CHO-K1 cells expressing NTSR1, pre-treated (10 min) with increasing concentrations (0, 1, 10, 32, and 100 µmol/L) of PP-001, as monitored by BRET^2. (d, e) NT-induced Gα_{13} dissociation and 1 and 2 recruitment in CHO-K1 cells pre-treated (10 min) with increasing concentrations (0, 1, 10, and 100 µmol/L) of NP-001 and PP-SCR-001 (e), as monitored by BRET^2. Luminescence was measured 30 min after pepducin stimulation, 20 min following NT(8-13) stimulation. Data represent the mean ± SEM of at least three independent experiments, tested in triplicate. Gamma radiation counts were normalized according to NT(8-13): data from untreated samples were set to 0% specific binding and data from NT(8-13) (1 µmol/L)-treated samples were set to 100% specific binding. BRET^2 ratios were normalized according to NT(8-13), in the "vehicle" pre-stimulation condition: data from vehicle-treated cells were set to 0% activation (or recruitment) and data from cells treated with NT(8-13) (1 µmol/L) were set to 100% activation (or recruitment). NS: non-stimulated (treated with buffer only).

in the efficacy (E_{max}) of NT to recruit both βarr1 and βarr2 was observed, reaching statistically significant levels at 10 µmol/L of PP-001 and above ($P < 0.05$). At 100 µmol/L of PP-001, NT-mediated recruitment was almost completely abolished, with inhibition of 91 ± 7% and 80 ± 20% for βarr1 and βarr2, respectively (Table S2; $P < 0.0001$ (βarr1), $P < 0.01$ (βarr2)). As with the G protein assays, we cannot conclude that the potency of NT to recruit βarrs was inhibited by PP-001, as the flattening of the NT curves led to a higher degree of uncertainty in the calculated EC_{50} values. Nevertheless, comparison of the pEC_{50} values between PP-001-treated and vehicle-treated conditions revealed a statistically significant rightward shift in NT potency, especially for βarr1 (Table S2; $P < 0.05$). Once again, the negative control pepducins NP-001 and PP-SCR-001 had no effect on the potency or efficacy of NT (Fig. 2d and e, Supporting Information Table S3); the pre-treated and vehicle-treated NT curves were superimposable in the G protein (Gα_{13}) and βarr assays. As an additional control, we tested palmitate in the same experimental paradigm to ensure that a high concentration of lipids inserted into the cell membrane could not alone disrupt NTSR1 signaling. NT-promoted signaling was not affected by palmitate pre-treatment (Table S3). Overall, these results suggest that, in addition to acting as a biased allosteric agonist of NTSR1, PP-001 acts as a NAM against the orthosteric NT binding and βarr signaling pathways.

3.3. PP-001 inhibits NT-induced receptor internalization

To support the results showing that PP-001 not only does not promote βarr recruitment to NTSR1 but also inhibits NT-induced βarr recruitment, we sought to evaluate the effect of PP-001 on NTSR1 receptor internalization. As it has been well established that βarr recruitment is a key step in the process of NTSR1 endocytosis[87–89], we expected PP-001 treatment to mirror the results described above (*i.e.*, not promote receptor internalization itself but inhibit NT-promoted receptor internalization). To

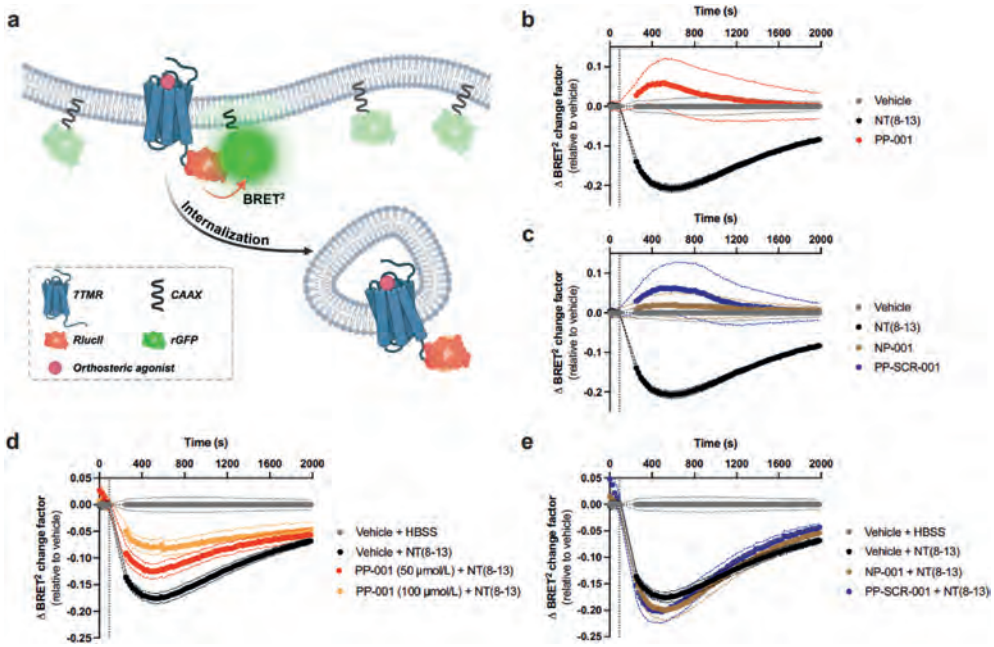

Figure 3 PP-001 does not promote NTSR1 receptor internalization on its own but inhibits NT-induced receptor internalization. (a) Principle of receptor internalization assay. Agonist-induced receptor endocytosis leads to a loss of $BRET^2$ signal, as the donor-tagged (RlucII) receptor is isolated from the acceptor-tagged, PM-localized CAAX-rGFP sensor. (b, c) Kinetic assays monitoring NTSR1 receptor internalization over a 30 min period in transiently transfected CHO-K1 cells, following stimulation with vehicle (HBSS, 1% DMSO), NT(8-13) (1 µmol/L), PP-001 (50 µmol/L), NP-001 (50 µmol/L) or PP-SCR-001 (50 µmol/L). (d, e) Kinetic assay monitoring NT(8-13) (1 µmol/L)-induced NTSR1 receptor internalization over a 30 min period, in transiently transfected CHO-hNTSR1 cells pre-stimulated (15 min) with PP-001 (50, 100 µmol/L), NP-001 (50 µmol/L), or PP-SCR-001 (50 µmol/L). Data represent mean ± SEM of four independent experiments, tested in duplicate. To determine a "$\Delta BRET^2$ change factor", each condition was normalized according to itself and corrected to vehicle: baseline data for each condition was set as a value of 1 and subtracted from vehicle (or vehicle + HBSS)-treated condition. Schema was created with Biorender.com.

monitor NTSR1 receptor endocytosis, we used a $BRET^2$ assay in which CHO-K1 cells were co-transfected with the donor-tagged NTSR1 receptor (hNTSR1-RlucII) and an acceptor-tagged plasma membrane marker (rGFP-CAAX)[59]. The principle of the assay is schematized in Fig. 3a; an internalization of the receptor into the cell is reflected by a loss in $BRET^2$ signal as the donor-tagged receptor becomes isolated from the membrane-bound acceptor sensor.

We first performed agonist type kinetic assays in which, following a baseline $BRET^2$ luminescence reading, CHO-hNTSR1 cells were stimulated with either the vehicle or a single concentration of NT(8-13) (1 µmol/L), PP-001 (50 µmol/L), NP-001 (50 µmol/L), or PP-SCR-001 (50 µmol/L). Luminescence was subsequently monitored over a 30-min period. As can be observed in Fig. 3b and c, NT(8-13) triggered a decrease in the $BRET^2$ change factor, which is consistent with receptor endocytosis. A maximum decrease of 0.21 ± 0.01 $BRET^2$ change factor was observed by 8.2 min post-treatment, followed by a slow return toward baseline. In contrast, PP-001 treatment did not produce any decrease. Rather, a slight increase was observed, although this was transient, highly variable between replicates, and also occurred in PP-SCR-001-treated cells. Compared to the vehicle, NP-001 did not trigger any change to the $BRET^2$ ratio.

Subsequently, we performed allosteric modulator type kinetic assays, in which CHO-hNTSR1 cells were pre-treated with the vehicle or pepducins for 10 min. As above, this step was followed by a baseline luminescence reading, stimulation with the vehicle or NT(8-13) (1 µmol/L), and a 30-min readout period. As can be observed in Fig. 3d, pre-treatment of cells with PP-001 effectively reduced the NT(8-13)-promoted decrease in $BRET^2$ ratio. Comparing the maximum decrease values in each condition, this corresponds to an inhibition of NT(8-13)-promoted NTSR1 endocytosis of 43 ± 9% (50 µmol/L) and 67 ± 7% (100 µmol/L). The control compounds NP-001 and PP-SCR-001 did not reduce NT(8-13)-promoted endocytosis (Fig. 3e). Along with the βarr recruitment data, these findings reinforce the classification of PP-001 as a NAM, capable of inhibiting NT-mediated βarr recruitment and NTSR1 receptor internalization in a concentration-dependent manner.

3.4. PP-001 may allosterically promote NTSR1−NTSR1 and NTSR1−APJ interactions

To further characterize PP-001-mediated actions *in vitro*, we sought to evaluate whether PP-001 treatment impacts NTSR1's ability to self-associate into homomers or to form heteromers with other 7TMRs. Indeed, it has been established that 7TMRs can assemble to form dimers and higher-order oligomers, particularly for obligate dimer Class C GPCRs, although the relevance of this process *in vivo* is still debated[90]. NTSR1, specifically, has been shown to homomerize in detergent solutions[91], in reconstituted phospholipid bilayer systems[92], and in HELA cells[93]. It has been proposed that this interaction is transient and follows a "rolling interface" model in which the protomers may adopt multiple configurations during their dimer lifetime[94].

To monitor NTSR1−NTSR1 interactions in live cells, we performed $BRET^2$ titration experiments in which CHO-K1 cells were transfected with a fixed quantity of donor-tagged receptor

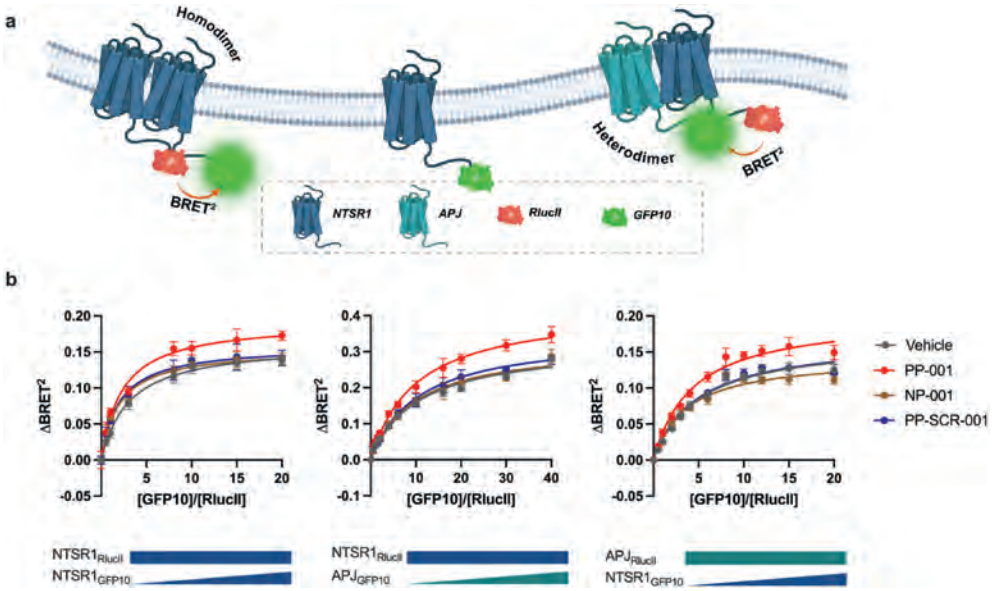

Figure 4 PP-001 promotes receptor-receptor interactions. (a) Principle of $BRET^2$ homo- and heteromerization assay. Formation of multimeric donor (RlucII) and acceptor (GFP10)-tagged receptor units leads to an increase in $BRET^2$ signal. (b) $BRET^2$ titration experiments monitoring receptor-receptor interactions in transiently transfected CHO-K1 ($NTSR1_{RlucII}$-$NTSR1_{GFP10}$) and HEK293 ($NTSR1_{RlucII}$-APJ_{GFP10}, APJ_{RlucII}-$NTSR1_{GFP10}$) cells treated with vehicle (HBSS, 1% DMSO) or pepducin series PP-001, NP-001, and PP-SCR-001 (100 μmol/L). In the $NTSR1_{RlucII}$-APJ_{GFP10} experiments (middle panel), cells were treated with 50 μmol/L of pepducin series. In these titration experiments, cells were transfected with fixed amounts of $7TMR_{RlucII}$ and increasing amounts of $7TMR_{GFP10}$; specific receptor-receptor interactions is evidenced by a saturation curve rather than a linear increase. Data represent mean ± SEM of three independent experiments, tested in duplicate. A one-way ANOVA followed by Dunnett's multiple comparisons test was performed on the $BRET_{50}$ and $BRET_{max}$ parameters derived from each curve. The resulting values are provided in Table S4. Schemas was created with Biorender.com.

(hNTSR1-RlucII) and increasing quantities of acceptor-tagged receptor (hNTSR1-GFP10) (Fig. 4a). In this experimental paradigm, specific receptor−receptor interactions are reflected by a $BRET^2$ increase that follows a saturation curve, whereas nonspecific interactions are reflected by a linear $BRET^2$ increase[95]. As shown in Fig. 4b (left panel), a clear saturation curve was obtained under vehicle-treated condition, indicative of constitutive dimerization of NTSR1 (conceivably, NTSR1 may also assemble into higher-order complexes, although studies suggest that NTSR1 predominantly forms dimers[91,92,94]). Treatment with pepducin PP-001 led to a significant upward shift ($P < 0.01$), corresponding to a 25 ± 1% increase in $BRET_{max}$ (100 μmol/L, left panel of Fig. 4b; Supporting Information Table S4). Interestingly, PP-001 did not affect the ratio of transfected GFP10/RlucII at which 50% $BRET^2$ was observed ($BRET_{50}$), suggesting that the pepducin may not increase the affinity of NTSR1 protomers for each other, but rather promote a configuration or rearrangement within the dimer that enhances the $BRET^2$ signal. Neither NP-001 nor PP-SCR-001 treatment (100 μmol/L) altered the $BRET^2$ saturation curve, compared to the vehicle-treated condition, supporting our hypothesis that the actions of PP-001 follow membrane tethering and are sequence-specific.

In addition to forming NTSR1−NTSR1 homomers, NTSR1 has been reported to form heteromers with several other 7TMRs, including the neurotensin receptor type 2 (NTSR2)[93,96], the dopamine receptor type 2 (D2R)[97,98], the kappa opioid receptor (KOPR)[99], and the apelin receptor (APJ)[100]. Here, we chose to monitor NTSR1−APJ interactions by performing similar $BRET^2$ titration experiments in HEK293 cells. To increase the robustness of our findings, we performed these experiments using both biosensor pairings: NTSR1-RlucII/APJ-GFP10 (Fig. 4b, middle panel) and APJ-RlucII/NTSR1-GFP10 (Fig. 4b, right panel). For one of these pairings (NTSR1-RlucII/APJ-GFP10), we reduced the pepducin concentrations to 50 μmol/L, to determine whether this lower concentration was sufficient to enhance heteromerization. As in the NTSR1-NTSR1 assays, we observed clear saturation curves in cells treated with the vehicle, indicating specific receptor-receptor interactions. Consistent with the homomeric assays, treatment with PP-001 resulted in a significant increase in the $BRET_{max}$ in both assays, representing an increase of 31 ± 3% ($P < 0.05$) and 28.0 ± 0.2% ($P < 0.05$) for NTSR1-APJ and APJ-NTSR1, respectively (Fig. 4b; Table S4). There was no significant change in the $BRET_{50}$ value for PP-001 compared to the vehicle-treated condition, and treatment with NP-001 or PP-SCR-001 did not significantly alter either parameter. Overall, these findings suggest that PP-001 promotes NTSR1 receptor homomer- and heteromer-forming processes.

3.5. PP-001 induces a sustained drop in blood pressure in rats

NTSR1 activation has been associated with various physiological effects that PP-001 may be able to modulate, notably hypotension. Indeed, NT's depressor effect on rat blood pressure was reported in the very first paper introducing NT[101], earning it the "tensin" portion of its name. Importantly, NT's hypotensive effects are thought to be primarily mediated by NTSR1 and not NTSR2, as NTSR2 is poorly expressed in vascular and cardiac tissues in both rats and humans[102,103], and the NTSR1-selective antagonist SR48692 has been shown to inhibit the NT-mediated hypotensive response[104,105].

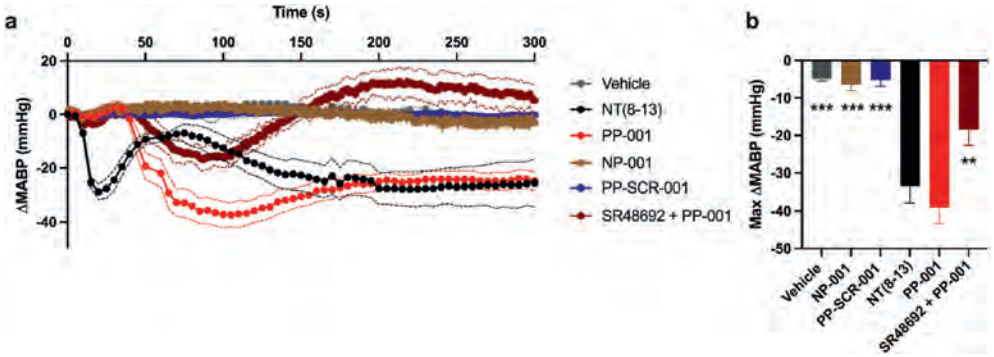

Figure 5 PP-001 induces a sustained drop in arterial blood pressure in rats. (a) Changes in mean arterial blood pressure (MABP) recorded in carotid-artery cannulated male Sprague−Dawley rats over a 5 min-period, following injection into the jugular vein of vehicle (saline, 5% DMSO), NT(8-13), PP-001, NP-001, or PP-SCR-001 at 55 nmol/kg doses. In the SR48692 + PP-001 condition, rats received the NTSR1-selective non-peptide antagonist SR48692 (1 mg/kg) 10 min prior to PP-001 (55 nmol/kg). (b) Maximal arterial blood pressure decreases (⊿MABP) recorded for each condition. Data represent mean ± SEM, $n = 4$ (NP-001, SR48692 + PP-001), $n = 5$ (vehicle, NT(8-13), PP-SCR-001), $n = 7$ (PP-001) rats. Data were statistically analyzed by a One-way ANOVA followed by Dunnett's multiple comparisons test, comparing each condition to PP-001-treated condition. ***$P < 0.001$; **$P < 0.01$.

To determine the hypotensive potential of these pepducins, we monitored mean arterial blood pressure (MABP) in carotid-artery-cannulated Sprague−Dawley rats, following intravenous injection of NT(8-13) and NTSR1-derived pepducins. As shown in Fig. 5a, intravenous administration of NT(8-13) (55 nmol/kg or 0.045 mg/kg) led to a triphasic response, characterized by an immediate initial decline, reaching −29 ± 3 mm Hg 20 s post-injection, a near-complete return to baseline (−7 ± 3 mm Hg at 75 s post-injection), followed by a second, slower decline that stabilized at −28 ± 6 mm Hg by 200 s post-injection. In contrast to NT's triphasic response, PP-001 at an equimolar dose (55 nmol/kg), after an initial 40-s delay, produced a potent and sustained drop in blood pressure, reaching a minimum of −37 ± 4 mm Hg by 105 s post-injection (Fig. 5a and b). A slow upturn ensued, but 300 s post-injection, MABP had stabilized at −25 ± 3 mm Hg. Importantly, neither NP-001 nor PP-SCR-001 induced hypotension in rats: mean maximum ΔMABP values were −7 ± 2 mm Hg and −5 ± 2 mm Hg, respectively, compared to −4.8 ± 0.7 mm Hg for the vehicle-treated control group. Finally, when the NTSR1 antagonist SR48692 (1 mg/kg) was pre-administered to rats 10 min prior to PP-001 (55 nmol/kg), the hypotensive effect of PP-001 was significantly reduced (54% reversal), reaching only −17 ± 4 mm Hg, supporting that the *in vivo* action of PP-001 is mediated by NTSR1.

3.6. PP-001's N-terminal RKK motif is critical to its cellular actions

To gain mechanistic insight into how PP-001 exerts its effects, and more specifically the relative importance of each amino acid side chain in the PP-001 peptide sequence, we synthesized a 13-pepducin series corresponding to an alanine scan of PP-001. To do so, the residues in positions 2 to 14 of PP-001 (corresponding to residues R90 to H102 of hNTSR1) were sequentially replaced by alanine residues (note that the residue in position 1 of PP-001, corresponding to A89 of hNTSR1, is already an alanine). The sequences of these pepducins are provided in Table 1. To characterize the impact of these substitutions on PP-001's biological activity, we used a label-free technique that measures the global response of a cell monolayer to ligand treatment, namely Electric Cell-substrate Impedance Sensing (ECIS). In this functional assay, cells are seeded onto cell culture plates incorporating gold-plated electrodes at the bottom of each well, through which an alternating electric current is passed. The resistance to the current's flow both across (transcellular) and between (paracellular) the cells is monitored. The ligand-induced dynamic mass redistribution (DMR) in the cell monolayer, which may include changes in morphology, cytoskeletal organization, and cell−substrate or cell−cell adherence, is accompanied by changes in electrical resistivity[60,106].

Here, the DMR kinetics of CHO-K1 cells stably expressing NTSR1 were monitored for 1 h following treatment with 10 μmol/L pepducin. We selected the 10-μmol/L concentration for pepducin testing, having previously found this concentration to be sufficient to promote a cellular response in a similar whole-cell integrated response assay[42] and wishing to maintain a low concentration to visualize early differences in the response profile. While the application of PP-SCR-001 did not induce any changes to electrical resistance, cell stimulation with PP-001 triggered an immediate increase that reached a near-plateau by 180 s (3 min), with a maximum change factor of 1.06 ± 0.01 by 1110 s (18.5 min) post-stimulation (Fig. 6). This increase was followed by a gradual decrease that intercepted the *x*-axis at 2700 s (45 min) post-stimulation. This response profile was similar, but not identical, to the resistivity traces induced by NT and NT(8-13) previously reported[60], in which NTSR1 activation was also associated with an increase in resistance.

Subsequently, each pepducin in the alanine scan series was tested, and their profiles were compared to those of PP-001. A color-coded representation of the impact of each substitution on the cellular response induced by PP-001 is provided in Fig. 6a, while the complete resistance traces are provided in Fig. 6b. As clearly shown, pepducins with substitutions at positions 2 and 3, [Ala^2]PP-001 and [Ala^3]PP-001, were completely inactive in this ECIS assay, with their traces being superimposable on those of the negative control PP-SCR-001. [Ala^4]PP-001 also produced a flat-line response up to 1770 s (29.5 min) post-stimulation, at which point a slow decrease in resistance occurred, culminating in a minimum factor of change value of 0.94 ± 0.04 at 3000 s (50 min) after stimulation. Overall, this suggests that the N-terminal RKK motif is critical for the biological activity mediated by PP-001, as

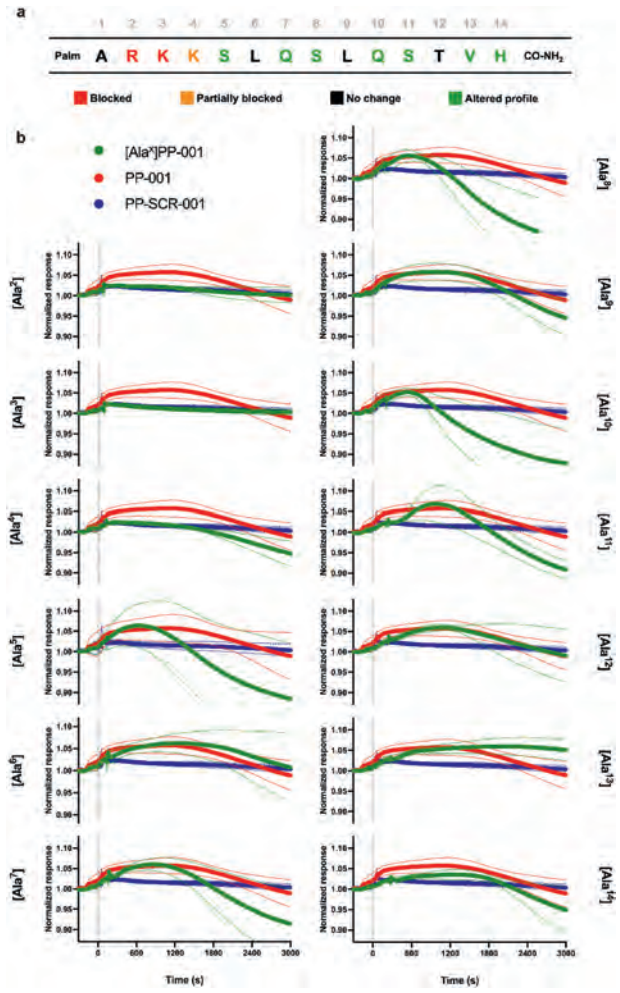

Figure 6 An alanine scan of PP-001 reveals critical residues for biological activity. (a) Color-coded representation of the effects of alanine substitutions on PP-001-induced biological activity. Alanine substitutions of the amino acids shown in red and orange resulted in a total or almost complete loss, respectively, of the pepducin-induced cellular response in an assay monitoring the dynamic mass redistribution (DMR) kinetics of CHO-hNTSR1 cells. For those shown in black, a response profile similar to that of PP-001 was observed; for those indicated in green, the response profile was altered. (b) DMR kinetics of CHO-K1 cells stably expressing NTSR1, treated with 10 μmol/L concentrations of PP-001, PP-SCR-001, or each of the PP-001 alanine scan pepducins. DMR was monitored by Electric Cell-substrate Impedance Sensing (ECIS) for 50 min post-stimulation. Data represent mean ± SEM, $n = 3$, tested in duplicate. Each condition was normalized to reflect a "normalized response" (or "change factor") relative to baseline resistance values (ohms).

changes in these residues completely or quasi-completely abolished the PP-001-induced cellular response. The importance of the RKK motif is further highlighted by the fact that a C-terminally truncated pepducin containing only the peptide sequence ARKKSL (PP-005) displays a signaling signature identical to that of PP-001 (Supporting Information Fig. S1). However, PP-005 was less effective than PP-001 in reversing nociceptive behaviors in a tonic pain model (formalin) in rats[42], which is why the full-length pepducin was retained for further characterization.

Of the remaining pepducins in the alanine scan series, three produced resistivity traces that were very similar to PP-001: [Ala^6], [Ala^9], and [Ala^{12}]PP-001. This suggests that L6, L9, and T12 are residues of minor structural importance to PP-001-mediated activity. In contrast, stimulation with the seven other pepducins led to substantially altered response profiles. With the exception of [Ala^{14}]PP-001, each produced an increase in amplitude resistance similar to that of PP-001, but with altered kinetics and, in many cases, a more marked decrease below the baseline. [Ala^5]PP-001, for example, reached its maximum (1.06 ± 0.03) at 600 s (10 min) post-stimulation, and then intercepted the baseline 1475 s (24.6 min) after stimulation, which is much earlier than for PP-001. The subsequent decrease in resistance reached levels of 0.88 ± 0.08 by 3000 s (50 min). [Ala^8] and [Ala^{10}]PP-001 displayed similar profiles to [Ala^5]PP-001, reaching their maximum values at 543 s (9.1 min) and 536 s (8.9 min) and intercepting the baseline at 1254 s (20.9 min) and 1087 s (18.1 min), respectively. In addition, the [Ala^7] and [Ala^{11}]PP-001 profiles are distinguished by an initial delay in response, as the increase in electrical resistance induced by these pepducins began around 300 s (5 min) and 420 s (7 min) post-treatment, respectively. Each trace reached its maximum (1.06 ± 0.02 and 1.07 ± 0.04) by 880 s (14.7 min) and 979 s (16.3 min) after treatment, respectively. As with [Ala^5], [Ala^8], and [Ala^{10}]PP-001, the baseline-to-baseline timeframe was much shorter for [Ala^7] and [Ala^{11}]PP-001 than for PP-001, extanding over a period of 25.4-min and 24.1-min period, respectively, compared to 45-min for PP-001. The subsequent decrease in resistance persisted below the baseline (change factors of 0.91 ± 0.9 and 0.91 ± 0.02, respectively, 3000 s post-treatment). As indicated above, the cellular response induced by 10 μmol/L [Ala^{14}]PP-001 was the only non-flatline trace that produced a lower amplitude response than PP-001, with a maximum change factor of 1.04 ± 0.01 by 1204 s (19.4 min) post-treatment and a return to baseline by 2227 s (37.1 min). Despite the lower amplitude, the kinetics observed resembled PP-001's trace. Finally, treatment with [Ala^{13}]PP-001 resulted in an increase in resistance that was maintained throughout the readout period. This increase first stabilized around 640 s (10.7 min) and then slowly increased to a maximum of 1.06 ± 0.02 by 1962 s (32.7 min). At the end of the readout (3000 s, or 50 min), the change factor was still above baseline (1.05 ± 0.03). Collectively, these substitutions highlight the importance of the N-terminal RKK motif for the activity of PP-001, although several sites may be of interest for further understanding the mechanisms of action of PP-001.

3.7. Alanine substitutions at positions 2 and 13 of PP-001 alter the pepducin's behavior in vitro and in vivo

Among the above series of pepducins, two were selected for further characterization: [Ala^2]PP-001 and [Ala^{13}]PP-001. In the case of the former, we sought to assess the extent to which the RKK motif is essential to PP-001, in particular whether the inactivity of [Ala^2]PP-001 observed with the ECIS assay extended to other *in vitro* and *in vivo* functional assays. We also selected [Ala^{13}]PP-001, as it was the only pepducin with a modified response profile for which the resistance-enhancing effect persisted longer than for PP-001; for all the others, the timeframe was shortened. We therefore sought to determine whether this altered response profile translated into increased potency and/or efficacy. Consequently, both pepducins were subjected to the same battery

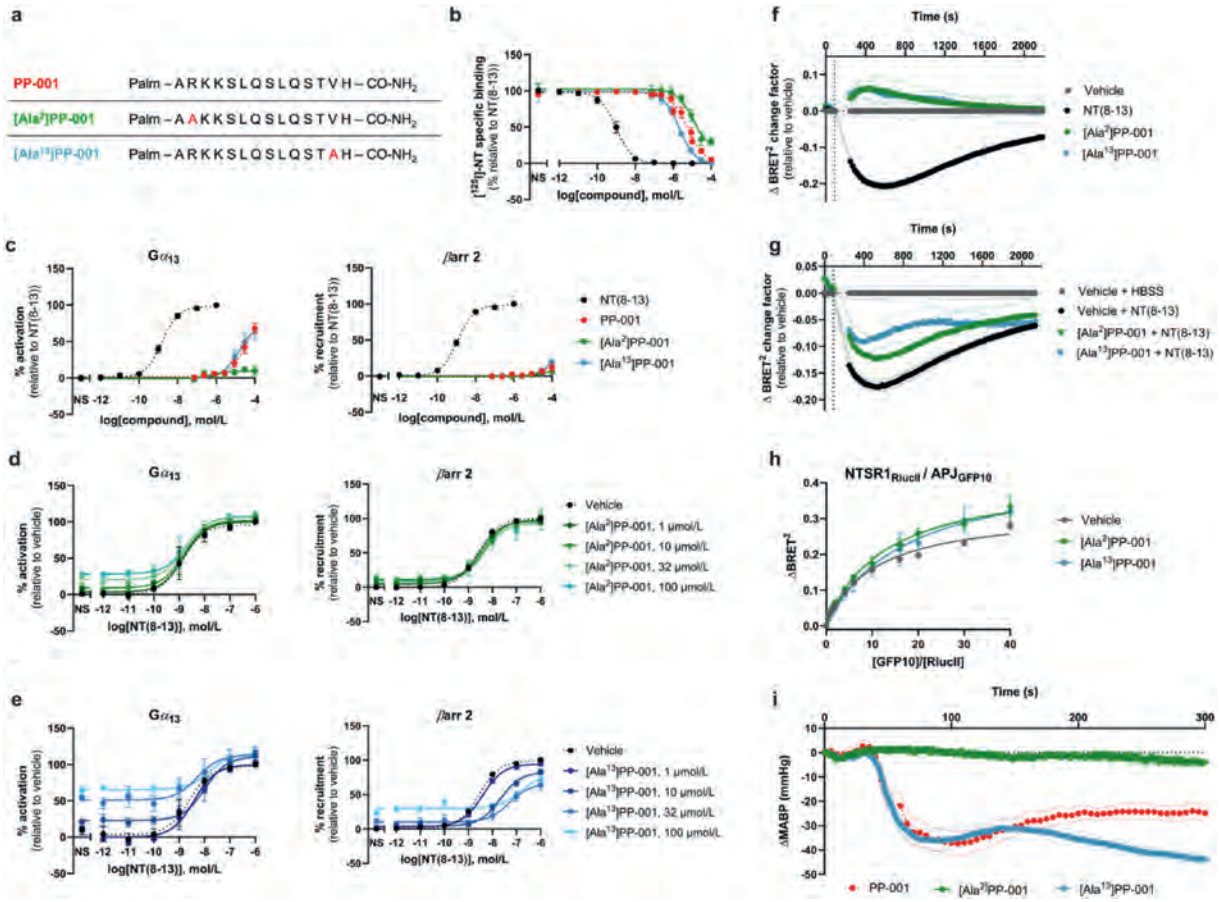

Figure 7 [Ala^2]PP-001 exhibits reduced biological activity compared to PP-001, whereas [Ala^{13}]PP-001 behaves similarly. (a) Table comparing the peptide sequences of PP-001, [Ala^2]PP-001, and [Ala^{13}]PP-001. Alanine substitutions are shown in red. (b) Displacement of ^{125}I-radiolabeled NT following incubation of CHO-hNTSR1 membranes with increasing concentrations of NT(8-13), PP-001 (for reference), [Ala^2]PP-001, and [Ala^{13}]PP-001. $n = 3$, tested in triplicate. (c) Gα_{13} protein dissociation and βarr2 recruitment, monitored by BRET^2, in CHO-K1 cells transiently expressing NTSR1, in response to increasing concentrations of NT(8-13), PP-001 (for reference), [Ala^2]PP-001, and [Ala^{13}]PP-001. $n = 4$, tested in triplicate. (d, e) NT(8-13)-induced Gα_{13} protein dissociation and βarr2 recruitment in CHO-K1 cells transiently expressing NTSR1, pre-treated (10 min) with fixed concentrations (0, 1, 10, 32, and 100 µmol/L) of [Ala^2]PP-001 (d) and [Ala^{13}]PP-001 (e), as monitored by BRET^2. $n = 4$, tested in triplicate. (f) NTSR1 internalization over a 30-min period, in response to treatment with vehicle (HBSS, 1% DMSO), NT(8-13) (1 µmol/L), [Ala^2]PP-001 (50 µmol/L), or [Ala^{13}]PP-001 (50 µmol/L), in transiently transfected CHO-K1 cells. $n = 4$, tested in duplicate. (g) NT(8-13) (1 µmol/L)-induced NTSR1 internalization over a 30-min period, in transiently transfected CHO-K1 cells pre-treated (15 min) with vehicle (HBSS, 1% DMSO), [Ala^2]PP-001 (50 µmol/L) or [Ala^{13}]PP-001 (50 µmol/L). $n = 4$, tested in duplicate. (h) NTSR1$_{RlucII}$-APJ$_{GFP10}$ interactions in HEK293 cells treated with vehicle, [Ala^2]PP-001 (50 µmol/L) or [Ala^{13}]PP-001 (50 µmol/L), as monitored *via* BRET^2 titration experiments. $n = 3$, tested in triplicate. (i) Blood pressure changes over a 5 min period recorded in carotid artery-cannulated male Sprague-Dawley rats, following injection into the jugular vein of PP-001 (for reference), [Ala^2]PP-001 or [Ala^{13}]PP-001 (55 nmol/kg), $n = 5$. Data represent mean ± SEM. BRET^2 luminescence signaling data. (c–e) Were recorded 30 min post-pepducin stimulation. NS: non-stimulated (treated with vehicle only).

of tests as those performed for PP-001; the sequences of each pepducin are provided in Fig. 7a. Overall, we observed a trend toward complete loss or significant negative shifts in activity for [Ala^2]PP-001, while [Ala^{13}]PP-001 tended to yield similar, sometimes slightly more potent, effects than PP-001 (Fig. 7b–i).

First of all, in the competitive radioligand binding assay, we observed noticeable negative and positive shifts in potency for the [Ala^2]PP-001 and [Ala^{13}]PP-001 displacement curves, respectively (Fig. 7b). Indeed, [Ala^2]PP-001 displaced radiolabeled NT with an IC$_{50}$ of 11 ± 5 µmol/L, while [Ala^{13}]PP-001 exhibited an IC$_{50}$ of 2.1 ± 0.5 µmol/L, contrasting with the IC$_{50}$ of PP-001 of 5.5 ± 0.8 µmol/L. Note that at 100 µmol/L, [Ala^2]PP-001 did not fully displace radiolabeled NT, but retained 30 ± 8% specific binding.

In BRET^2 agonist signaling assays (Fig. 7c), [Ala^2]PP-001 led to minimal Gα_{13} protein dissociation (10 ± 7% activation at 100 µmol/L *vs.* 68 ± 7% activation for PP-001), whereas [Ala^{13}]PP-001 exhibited allosteric agonist activity similar to that of PP-001 (64 ± 11% activation at 100 µmol/L). Like PP-001, none of the alanine-substituted pepducins triggered significant recruitment of βarr2 to NTSR1. In allosteric modulator-type assays (Fig. 7d and e, Supporting Information Table S5), [Ala^2]PP-

001's inhibitory effect on NT(8-13) signaling was significantly reduced compared to PP-001. Indeed, in the $G\alpha_{13}$ protein signaling assay, the EC_{50} and E_{max} values of NT(8-13) were not significantly altered by [Ala^2]PP-001. Likewise, [Ala^2]PP-001 did not induce any reduction in E_{max} of NT(8-13) in the βarr2 assay (100 ± 20% recruitment at 100 μmol/L [Ala^2]PP-001 *vs.* 20 ± 20% for PP-001). As with PP-001, pre-treatment of CHO-hNTSR1 cells with [Ala^{13}]PP-001 resulted in a baseline increase of 64 ± 6% activation in the $G\alpha_{13}$ assay, consistent with its allosteric agonist action and induced a slight negative shift in EC_{50}. In the βarr2 assay, there was a statistically significant shift in both the potency and efficacy of NT(8-13), with a maximum 54 ± 16-fold ($P < 0.01$) increase in EC_{50} values and a maximum 36 ± 7% inhibition ($P < 0.01$) of the E_{max}.

In assays monitoring NTSR1 receptor internalization, neither [Ala^2]PP-001 nor [Ala^{13}]PP-001 triggered a decrease in BRET^2 at 50 μmol/L, as expected given their lack of agonist activity in the βarr2 recruitment assay (Fig. 7f). However, both pepducins, but particularly [Ala^{13}]PP-001, were able to inhibit NT(8-13)-triggered NTSR1 endocytosis (Fig. 7g). Indeed, the decrease in the BRET^2 signal relative to vehicle-treated cells observed after 1 μmol/L NT(8-13) was inhibited by 33 ± 19% and 50 ± 8% by 50 μmol/L [Ala^2]PP-001 and [Ala^{13}]PP-001, respectively. In comparison, pre-treatment with 50 μmol/L PP-001 resulted in a 43 ± 9% ($P < 0.05$) inhibition of NTSR1 endocytosis. The inhibition mediated by [Ala^2]PP-001 was unexpected, given the absence of NT(8-13)-mediated βarr2 recruitment inhibition observed in the signaling assays. Nevertheless, the inhibitory effect of [Ala^2]PP-001 was more moderate than that of PP-001.

In Fig. 7h, the effect of 50 μmol/L [Ala^2]PP-001 and [Ala^{13}]PP-001 on NTSR1-APJ heteromer interactions was monitored using the hNTSR1-RlucII and hAPJ-GFP10 biosensor pairing. In both cases, an upward shift of the BRET^2 saturation curve was observed. Compared to vehicle-treated cells, treatment with [Ala^2]PP-001 and [Ala^{13}]PP-001 led to a significant increase in $BRET_{max}$, (corresponding to an increase of 17 ± 7% and 14 ± 7%, respectively), which was lower than the 31 ± 3% increase observed with PP-001. The $BRET_{50}$ for each curve was 12 ± 1 and 17 ± 3, respectively, representing a statistically significant ($P < 0.05$) increase compared to that of vehicle-treated cells (10.3 ± 0.3) in the case of [Ala^{13}]PP-001.

Finally, both pepducins were administered intravenously to Sprague−Dawley rats to determine their hypotensive potential, at equimolar doses to PP-001 (55 nmol/kg) (Fig. 7i). Despite the biological activity demonstrated by [Ala^2]PP-001 in several of the above assays, no change to MABP was observed. In contrast [Ala^{13}],PP-001 induced a potent and sustained drop in blood pressure, initially following the same profile as PP-001, but diverging at the 140-s time-point. The same 40-s delay in response was observed for [Ala^{13}]PP-001 as for PP-001, followed by a rapid blood pressure decline, descending to −36 ± 4 mm Hg by 93 s post-administration. There was a brief stabilizing period, with a slow upturn toward baseline that reached −31 ± 4 mm Hg at 140 s. Unlike PP-001, this phase was succeeded by a second slow decline. By the end of the experiment (300 s post-administration), we recorded a ΔMABP of −44 ± 2 mm Hg, which is 19 ± 5 mm Hg lower than that of PP-001 at the same time-point. Altogether, these data highlight the importance of the lysine in position 2 for PP-001 activity and suggest that the valine at position 13 may be an interesting starting point for future structure-activity studies seeking to increase the pepducin's potency.

3.8. PP-001 binds directly to the rat NTSR1 receptor

As shown in Fig. 2, PP-001 inhibited the specific binding of NT(8-13) and allosterically modulated NTSR1 signaling, thereby confirming the pharmacological action of PP-001 on NTSR1. To further investigate the mechanism of action of PP-001 on NTSR1, we monitored the direct interaction between PP-001 and the receptor *in vitro* using a *N*-[4-(7-diethylamino-4-methyl-3-coumarinyl)phenyl]maleimide (CPM)-based stability assay on purified recombinant NTSR1[66]. This assay has been used to solve the mechanism of ligand binding to membrane proteins[66,107]. Briefly, this CPM stability assay monitors the impact of ligand binding on heat-induced denaturation of a receptor. GPCR purification is a challenge due to their inherent lack of *in vitro* stability. As such, protein engineering is commonly used to obtain stable 7TMR eluate. We therefore took advantage of two previously described engineered NTSR1 constructs (NTSR1-3 and NTSR1−22) used in structural biology studies (Supporting Information Figs. S2 and S3)[62] to measure the thermostability of NTSR1 in the presence of vehicle, NT(8-13) and PP-001 (Fig. 8) (The full list of mutations in the NTSR1−22 construct can be found in Table S6). For the two purified constructs NTSR1−3 and NTSR1−22, we found that NT(8-13) increased the resistance of NTSR1 to heat-induced denaturation, as indicated by the rightward shift of the thermodenaturation curve relative to the vehicle-treated sample (Fig. 8a and b). The extent of the shift could be quantified by the melting temperature (T_m), defined as the temperature at the maximum of the curve's first derivative (Fig. 8c and d). We found that NT(8-13) stabilized NTSR1 by approximately 6 °C for both constructs compared to the vehicle-treated receptor. In contrast, treatment with PP-001 decreased the heat resistance of both NTSR1 constructs by approximately 3−4 °C, as shown by a left-shift in the thermodenaturation curves. Accordingly, the change in Tm for both NT(8-13) and PP-001 indicates a direct binding of the ligands to purified NTSR1. Moreover, the opposite effect of NT(8-13) and PP-001 binding on NTSR1 stability suggest that they have a distinct mechanism of ligand action on the receptor, consistent with the allosteric efficacy observed for PP-001 on NTSR1-induced NT(8-13) signaling (Fig. 2b and c).

3.9. Substitutions of NTSR1 ICL residues impede PP-001 activity

Having gathered evidence supporting a direct interaction between the pepducin and the receptor, we sought to elucidate the PP-001/NTSR1 binding site, with a specific focus on the ICL regions. To do so, we relied on receptor mutagenesis techniques. We introduced a series of sequential alanine mutations into a human HA-tagged NTSR1 construct. Our strategy for this first attempt was to "scan" the ICL domains five alanine residues at a time, with the aim of identifying mutants against which PP-001's activity would be altered. Since the human NTSR1 receptor has four ICL sequences spanning 14 (ICL1: A89-H102), 20 (ICL2: E165-R184), 44 (ICL3: A260-R303), and 54 (C-term: N365-Y418) amino acids, as delineated by Uniprot (ID: P30989), 27 mutant constructs were generated (specific sequences can be found in Table S7). Note that in positions where an alanine was already expressed endogenously, it was simply conserved in the sequence.

We first verified the cell surface expression of the mutants by an enzyme-linked immunosorbent assay (ELISA) performed on transiently transfected HEK293 cells (Fig. 9a). Our results

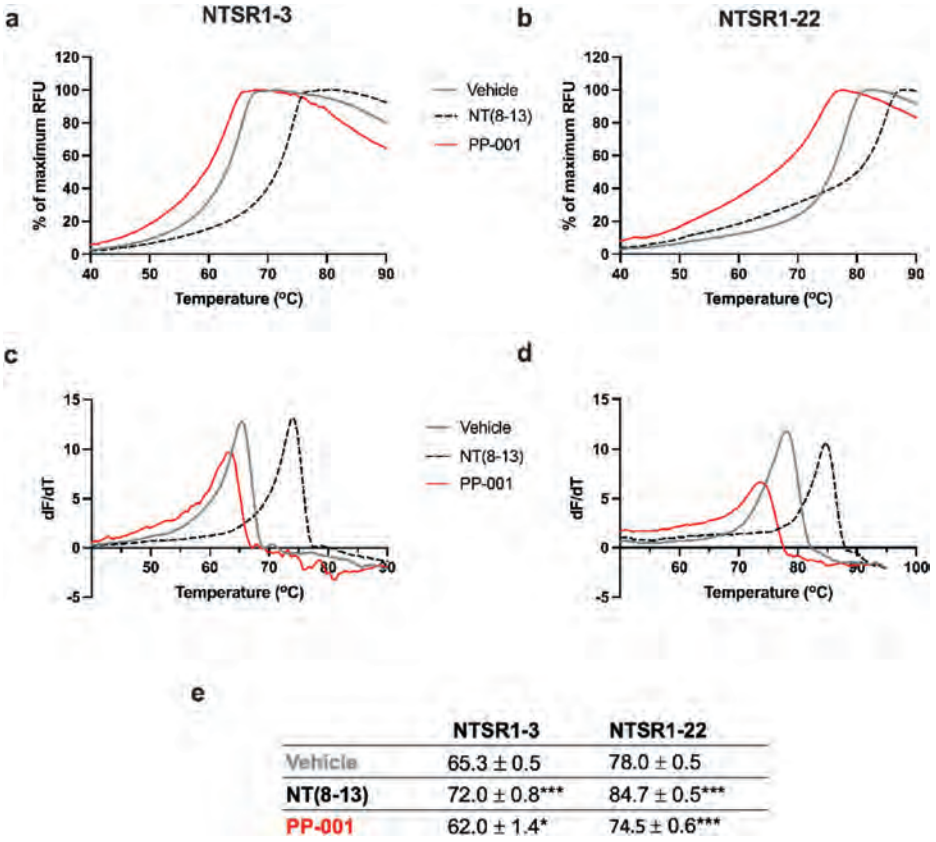

e

	NTSR1-3	NTSR1-22
Vehicle	65.3 ± 0.5	78.0 ± 0.5
NT(8-13)	72.0 ± 0.8***	84.7 ± 0.5***
PP-001	62.0 ± 1.4*	74.5 ± 0.6***

Figure 8 PP-001 binds to NTSR1. Representative CPM thermodenaturation curves of purified (a) NTSR1-3 or (b) NTSR1-22 in the presence of ligands or vehicle. (c, d) First derivative of the CPM thermodenaturation curves presented in (a) and (b), respectively. (e) Table of the T_m values determined from vehicle, NT(8-13) and PP-001 conditions. The data are expressed as a mean ± SEM of 3 independent experiments in duplicate. Statistical significance is determined by a one-way ANOVA followed by a Dunnett's *post hoc* analysis. ***P-value < 0.001; and *P-value < 0.05.

revealed that 17 mutants out of 27 were fully expressed, with expression levels greater than or equal to 100% compared to the wild type (WT) receptor. Seven mutants (Mutants 2, 5, 8, 14, 16, 17, and 20) had middling receptor expression levels, ranging from 46 ± 20% (Mutant 8) to 77 ± 20% (Mutant 20). Four were found to be poorly expressed (Mutants 1, 4, 18, and 19), with levels below 25% cell surface expression. Mutant 18 was the least expressed, at 11 ± 5% expression. Thus, in the following assays, the experimental conditions were optimized for each expression group to ensure a valid readout.

Here, we chose to test the WT receptor and the 27 mutants in the radioligand binding assay. The aim was to compare the inhibitory activity of PP-001 on the orthosteric NT binding at each mutant (relative to NT(8-13)) with that of the WT receptor. Fig. 9b shows the results obtained at 10 μmol/L PP-001. For 22 of the 27 mutants, PP-001 was found to inhibit [^{125}I]-NT binding to a similar extent as the WT condition. Interestingly, in the case of Mutants 2, 16, 17, 19, and 20, a greater amount of bound radioactivity was retained; in other words, the inhibitory effect of PP-001 on NT binding was partially reversed. In contrast to the 32 ± 4% specific binding retained at the WT receptor, the retained specific binding levels were 56 ± 6% (Mutant 2), 55 ± 5% (Mutant 16), 66 ± 3% (Mutant 17), 82 ± 9% (Mutant 19), and 57 ± 7% (Mutant 20). The locations of these mutations on NTSR1 are presented in the snake plot in Fig. 9c; they correspond to alanine substitutions in the ICL1 (Mutant 2), ICL3 (Mutant 16), and C-terminal tail (Mutants 17, 19, and 20) sequences of NTSR1. It should be noted that Mutants 19 and 20 are found within the H8 domain, while Mutant 17 is adjacent to H8. Unfortunately, no reliable data could be obtained for the 5 remaining mutants (1, 4, 5, 8, and 18).

In Fig. 9d–f, the full concentration–response curve data for both NT(8-13) and PP-001 are shown for the five highlighted mutants, along with the specific mutation sequences. The curves for the other 17 mutants are presented in Supporting Information Fig. S4. The IC_{50} and maximum inhibition values extracted from these curves can be found in Supporting Information Table S8. As can be seen, while the NT(8-13) curves for each mutant are superimposable on those for WT, the PP-001 curves are slightly but consistently shifted to the right. For Mutants 2 and 16, this represents a nearly three-fold shift in IC_{50}: 14 ± 2 and 13 ± 2 μmol/L, respectively, compared to 5.3 ± 0.5 μmol/L for the WT receptor. For Mutant 17, this shift is slightly more pronounced (23 ± 3 μmol/L). However, the greatest shift in affinity was observed for Mutant 19, with a shift of 70 ± 30 μmol/L. Interestingly, in the case of Mutant 20, the rightward shift of the PP-001 curve was more subtle (9 ± 3 μmol/L), but PP-001's inhibition of NT binding at 100 μmol/L was no longer complete. Instead, 24 ± 6% of the specific [^{125}I]-NT binding was still retained. Together, these data suggest that the PP-001/NTSR1

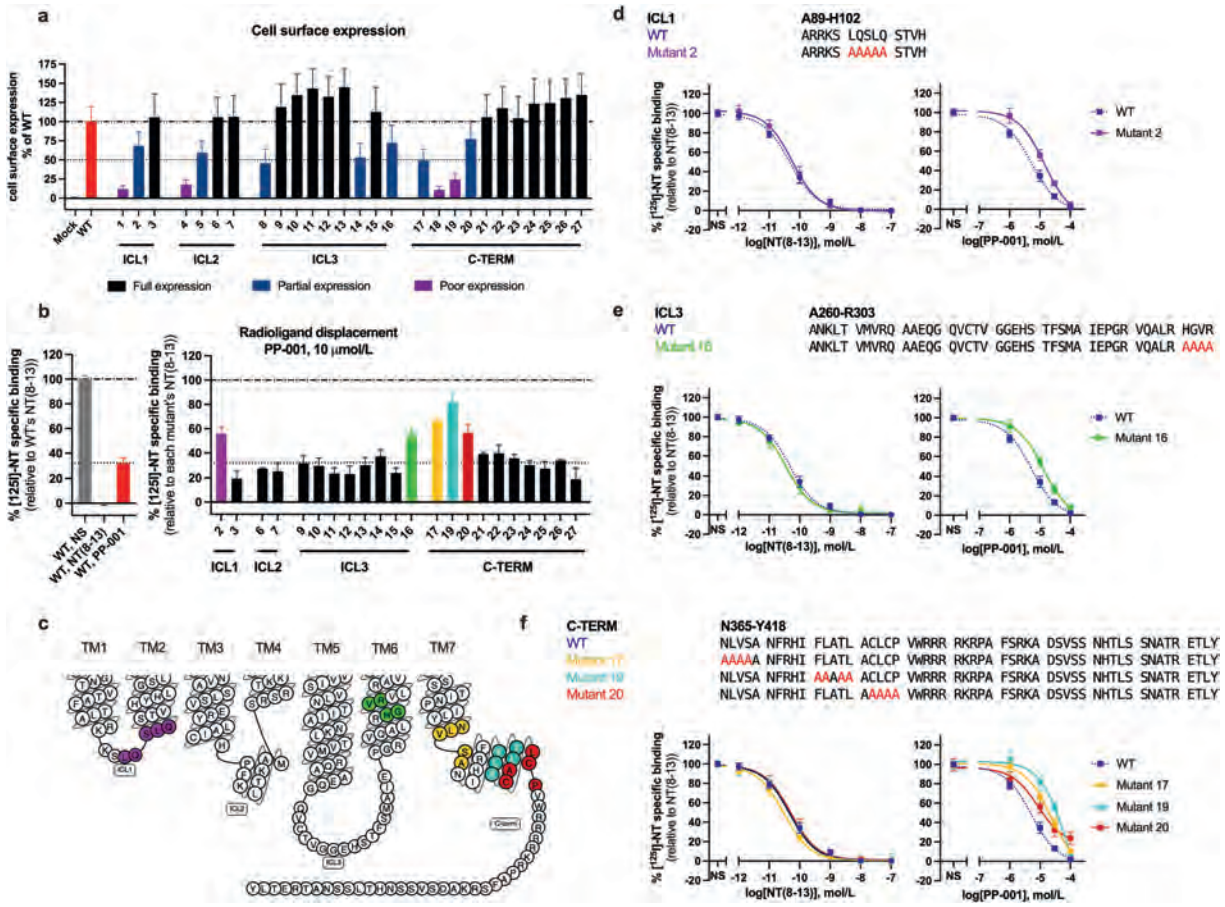

Figure 9 Alanine substitutions in NTSR1 ICL domains impede PP-001-driven inhibition of NT binding. (a) Cell surface expression of the HA-hNTSR1 WT receptor and the derived ICL mutant constructs (Mutants 1−27) in transiently transfected HEK293 cells, as determined by ELISA. Data was normalized to WT (set as 100% expression) and mock (set as 0% expression) conditions. $n = 3$, tested in duplicate. (b) Displacement of ^{125}I-radiolabeled NT by 10 µmol/L PP-001 in HEK293 cell membranes transiently transfected with the HA-hNTSR1 WT receptor (left) or the ICL mutant constructs (right). No reliable results could be generated with mutants 1, 4, 5, 8, and 18. Mutants represented in color (2, 16, 17, 19, 20) were found to retain greater binding of [^{125}I]-NT. $n = 2$, tested in duplicate. (c) Snake plot of the human NTSR1 receptor, cropped to ICL domains. Substituted residues in Mutants 2, 16, 17, 19 and 20 are identified in color. (d−f) Displacement of ^{125}I-radiolabeled NT following incubation of transiently transfected HEK293 membranes with increasing concentrations of "cold" NT(8-13) (left) or PP-001 (right). Data for the WT condition are compared to mutants in the ICL1 (Mutant 2, d), ICL3 (Mutant 16, e) and C-terminal (Mutants 17, 19, and 20, f) regions. Sequences of the ICL domains with relevant mutations are presented above each graph; alanine residue substitutions are shown in red. $n = 2$, tested in duplicate. Data represent mean ± SEM. Radioactivity data were normalized according to NT(8-13) (set as 100% specific binding) and untreated cells (set as 0% specific binding) for each individual mutant.

binding site may incorporate several ICL regions, but that H8 in the C-terminal domain could be a particularly interesting area.

3.10. Docking of PP-001 to the intracellular domains of NTSR1

To delineate the intracellular binding site of PP-001 on NTSR1, we docked the pepducin onto an MD-equilibrated model of the NT(8-13)−bound receptor embedded in a POPC bilayer, keeping NT(8-13) fixed within the orthosteric pocket. Across the top-ranked poses, PP-001 consistently localized to the cytoplasmic surface, spanning the TM7-H8 bend and the adjacent ICL rim. In the representative configuration, the peptide backbone lay approximately parallel to the membrane plane, with the *N*-palmitoyl chain positioned along the membrane-facing side of H8 (Fig. 10a). This orientation enables extensive interaction with residues across the H8 hinge and the ICL1/ICL3 interface.

Mapping the experimental mutational scan onto the docked interface recapitulated the graded phenotypes observed in functional assays. Mutation with ICL1 (Mut 2) and the ICL3 edge (Mut 16) corresponded to peripheral contacts whose alanine substitutions modestly right-shifted PP-001 potency and increased NT retention at 10 µmol/L (Fig. 10b and c). The H8-proximal hinge (Mut 17) aligned with a denser contact patch, producing a more pronounced right-shift, while mutations at the H8 core (Mut 19−20), coinciding with the highest-persistence contacts, elicited the strongest functional attenuation, including incomplete displacement at high PP-001 concentrations (Mut 20).

Together, the docking and mutational data define an H8-centric intracellular binding mode for PP-001 that is compatible with G-protein-competent conformations but encroaches on the β-arrestin engagement footprint. This model also potentially rationalizes why PP-001 binds directly to NTSR1 while reducing

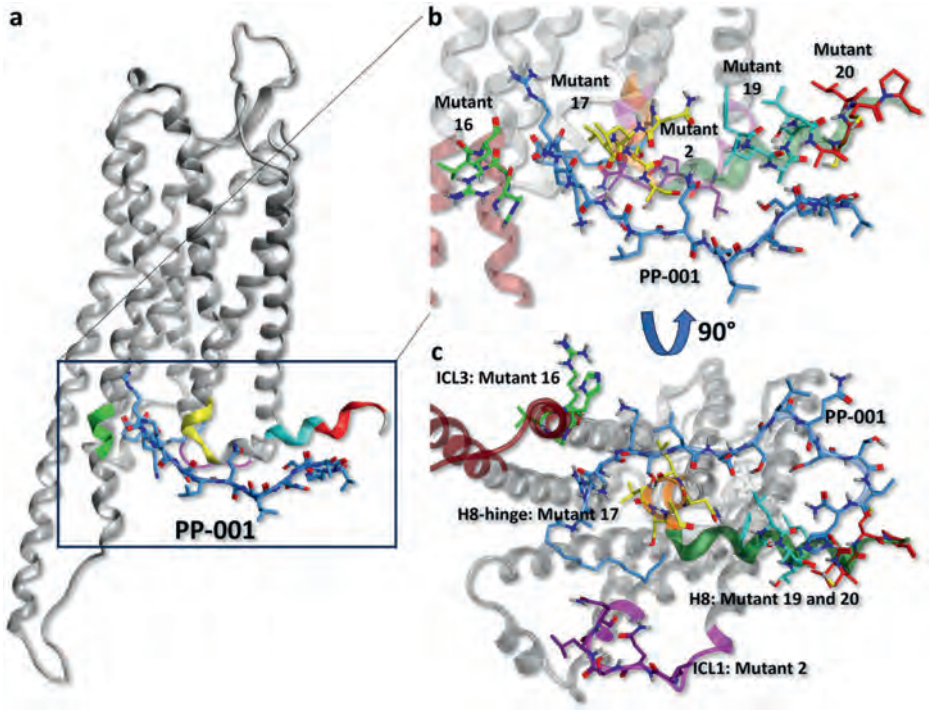

Figure 10 Docking of PP-001 to the intracellular domains of NTSR1. (a) Overall view of NTSR1 showing the lowest-energy docking pose of PP-001 (blue) and the positions of residues corresponding to mutants with altered PP-001 activity: Mutant 2 (pink), Mutant 16 (green), Mutant 17 (yellow), Mutant 19 (cyan), and Mutant 20 (red). (b) Close-up of the intracellular region of NTSR1 highlighting the proximity of PP-001 to the identified mutant sites. Ribbon colors represent structural domains: helix 8 (H8, green), intracellular loop 1 (ICL1, pink), intracellular loop 3 (ICL3, brown), and helix 7 C-terminal extension/H8 transition (orange). (c) Intracellular bottom view obtained after a 90° rotation, illustrating the spatial distribution of residues surrounding the PP-001 binding site.

receptor thermostability relative to NT(8-13). By engaging the H8 hinge and adjacent ICL surface, the pepducin appears to stabilize an intracellularly open, less tightly packed receptor state, diminushing apparent orthosteric peptide affinity, yet favoring G-protein coupling over β-arrestin recruitment. The correspondence between contact density in the model and the experimental rank order of effects (Mutant 19 $>$ Mut17 $\approx$ Mut20 $>$ Mut2 $\approx$ Mut16) supports this structural interpretation, highlighting H8 as the primary anchoring surface with ICL1/ICL3 providing secondary stabilization. Overall, these results position PP-001 within a mechanistic class of intracellular, H8-engaging pepducins that act as biased allosteric modulators. The resulting structural framework offers a foundation for targeted mutational scanning across H8 and for rational optimization of the pepducin's N-terminal motif and lipid anchor.

4. Discussion

In the present study, we characterized the modulatory effects of PP-001, a pepducin derived from the first intracellular domain of NTSR1, to elucidate how this class of molecules regulates receptor function. Our results show that this lipidated cell-penetrating peptide acts as a biased allosteric agonist, selectively activating G-protein signaling, promoting receptor oligomerization, and inducing potent hypotensive effets. PP-001 also behaves as a NAM of NTSR1, reducing the receptor's ability to bind to its natural orthosteric ligand and inhibiting NT-induced recruitment and receptor internalization. Finally, we also identified a key N-terminal motif required for PP-001 activity and highlighted the receptor's helix 8 domain as a likely site of pepducin−receptor interaction.

In vitro assays revealed that PP-001 preferentially activates G protein pathways while inhibiting NT binding, an uncommon finding, as most reported pepducins have little or no impact on orthosteric ligand binding. Notably, β2AR-derived pepducins (ICL1-9, ICL3-8, and ICL3-9)[6,7] and the CXCR4-derived pepducin ATI-2341 [4] showed negligible interference with ligand binding. Likewise, the PAR4-derived pepducin P4pal-10 inhibited FPR2-driven responses in neutrophils without directly competing for ligand binding[108]. To our knowledge, only F1pal-16 and F2pal-10 targeting FPR2 displayed competitive behaviors[19−21]. Although we cannot rule out some direct competition at the extracellular site, the absence of effect with the non-palmitoylated NP-001 peptide supports an intracellular allosteric mechanism. Rather, we believe that the pepducin, receptor, and ligand form an allosteric system in which they act respectively as modulator, conduit, and guest (to use Kenakin's terminology[109]), where PP-001 binding induces receptor conformations that alter NT(8-13) activity and *vice versa*.

PP-001's dual agonist/NAM behavior is unusual but parallels findings with urotensin receptor-derived pepducins (hUT-Pep2 and [Trp^1, Leu^2]hUT-Pep3), which activate Gα_i and Gα_{13} while inhibiting urotensin II-driven Gα_{12} signaling and aortic ring contractions[24]. The β2AR-derived ICL3-9 pepducin is another example of such mixed modulation[6,7]. These results highlight the complex signaling profiles achievable by intracellular allosteric modulators that selectively bias GPCR pathways[110]. The lack of

PP-001-induced NTSR1 endocytosis further supports its G protein-bias. Unlike NT(8-13), which promotes receptor internalization, both PP-001 and the scrambled control, in agonist mode, produced only a slight transient $BRET^2$ increase, likely due to pepducin's insertion into the cell membrane. In antagonist mode, PP-001 inhibited NT-induced endocytosis similarly to the $G\alpha s$-biased ICL3-9 pepducin[6], which enhances cAMP signaling while preventing isoproterenol-promoted β-arrestin recruitment and β2AR internalization. Such effects may prolong surface receptor availability and sustain G protein-mediated signaling. Collectively, these data indicate that PP-001 induces NTSR1 conformations that (1) favor G protein signaling over recruitment (biased allosteric agonism) and (2) impede NT binding and signaling (NAM behavior), possibly *via* altered receptor thermodynamic stability. Although PP-001 did not inhibit NT-induced G protein activation in our assays, this may have been masked by its own agonist behavior and ability to prevent NTSR1 endocytosis.

We also demonstrated for the first time that PP-001 promotes the formation of NTSR1−NTSR1 homomers and NTSR1−APJ heteromers, an effect not observed with the CXCR4-derived pepducin ATI-2341[13]. Although receptor dimerization has long been discussed in the context of pepducin research (indeed, since the seminal 2002 study by Covic et al.[1]), the notion that pepducins might mimic or stabilize protomer−protomer interactions remains largely speculative. If pepducins can indeed form "pseudo-dimers" with their target receptors, they may be tapping into signaling features that are unavailable to monomeric receptor units. In the case of PP-001, it remains unclear whether the observed effect reflects the *de novo* formation of NTSR1 dimers (yielding a potential "pseudo-trimer") or a conformational rearrangement within pre-existing dimers that enhances the $BRET^2$ signal. In either scenario, our findings support a direct receptor-pepducin interaction and underscore a distinctive feature of pepducin pharmacology that differentiates them from conventional extracellular ligands.

In vivo, PP-001 produced a potent and sustained hypotensive response, consistent with NTSR1 activation[111]. Unlike NT(8-13), which elicits a triphasic response driven by mast cell degranulation and the release of histamine and catecholamine[112,113], intravenous injection of PP-001 induced a more pronounced and longer-lasting decrease in blood pressure. Given the difference in potency between NT(8-13) and PP-001, the intensity of this response was somewhat unexpected. If the hypotensive effect arises primarily from G protein-mediated signaling at NTSR1, as suggested by PP-001's biased signaling profile, it is conceivable that simultaneous inhibition of endogenous NT-signaling and NTSR1 internalization potentiates the G protein-dependent hypotensive response. An additional factor may involve the distinct pharmacokinetic behaviors of pepducins. Unlike NT(8-13), which rapidly activates NTSR1 upon systemic administration and triggers immediate release of histamine, PP-001 must first insert into the plasma membrane before engaging the receptor. This likely results in a slower and more prolonged activation of NTSR1, potentially leading to a delayed or sustained histamine release that catecholamines cannot readily counteract. Other properties of PP-001, such as the lack of receptor desensitization or the promotion of multimeric receptor assemblies, may further contribute to this prolonged hypotensive effect.

Importantly, the NTSR1 antagonist SR48692, which occupies binding domains partially overlapping those of NT, abolished the hypotensive action of PP-001, confirming that pepducin's effect was mediated by NTSR1. Interestingly, the small-molecule modulator SBI-553, another NTSR1 allosteric ligand, displays an opposite signaling bias: it acts as a -biased allosteric agonist, selectively inhibiting NT-induced G protein signaling while potentiating estin pathways (PAM behavior)[114]. Structural studies using cryo-EM have shown that SBI-553 binds within the receptor's intracellular cavity[115,116]. In line with its signaling bias, SBI-553 does not induce hypotension in mice[117], contrasting sharply with the robust hypotensive effect of PP-001. Overall, these results reinforce the concept of allostery, whereby intracellular modulators such as pepducins can influence orthosteric ligand binding and signaling, while orthosteric agonists or antagonists may reciprocally modulate the actions of intracellular allosteric ligands.

Alanine scanning identified a critical N-terminal RKK motif in PP-001, as substitution of Arg2 with alanine ($[Ala^2]$PP-001) abolished activity across multiple *in vitro* and *in vivo* functional assays. This agrees with other pepducin studies showing the importance of positively charged residues such as R and K for pepducin activity. For example, Forsman et al.[20] reported complete inactivity of the FPR2-derived pepducin $F2pal_{10}$ when lysine at position 5 (K5) is replaced with A, N, or Q, but regains function when replaced by a positively charged arginine residue. Similarly, the activity of P1pal-19 (a PAR1 mimic) was impaired following substitutions at R16, and to a lesser extent at R11 and K13. For pepducins, the precise contribution of such key residues often remains ambiguous, whether they primarily facilitate membrane insertion and the flip-flop process, mediate receptor (and/or its effectors) interactions, or fulfill a combination of both functions. It is indeed conceivable that the positively charged lysine residues facilitate membrane translocation of PP-001, as positive charges have been shown to increase peptide permeability[118]. This is particularly true for cell-penetrating peptides[119], where polyarginine sequences have proven to be especially effective carriers[120]. Nevertheless, given that multiple alanine substitutions produced distinct alterations in impedance response profiles, the relationship between PP-001's primary structure and its complex modulation of NTSR1 signaling remains intricate and warrants further investigation.

Finally, we used a thermal denaturation assay to provide direct evidence of PP-001 binding to purified NTSR1 protein. While few studies have successfully demonstrated pepducin/receptor interactions, several methodologies have been reported: Janz et al.[4] used photochemical cross-linking approach to reveal direct binding between CXCR4 and ATI-2341, Carr et al.[6] monitored pepducin-induced conformational changes in β2AR using monobromobimane-labeled receptors, and Zhang et al.[121] employed biotinylated peptides to immunoprecipitate PAR1. In our assays, PP-001 induced a significant leftward shift in the melting temperature (T_m) of both NTSR1−3 and NTSR1−22 constructs, consistent with direct interaction. Interestingly, this shift contrasts with the effect of NT(8-13), suggesting that PP-001 stabilizes distinct, less thermodynamically stable receptor conformations. The observed reduction in NTSR1 thermal stability upon PP-001 binding may reflect a transition toward a more dynamic and flexible conformational ensemble, potentially associated with pepducin-induced receptor oligomerization. Given that NTSR1 can form homodimers through multiple interfaces[122], it remains to be determined whether the reduced thermostability arises from specific effects on dimerization interfaces or from broader allosteric modulation of receptor dynamics[123]. Despite these uncertainties, our findings provide strong evidence for direct pepducin−receptor interaction and offer mechanistic insights into how intracellular allosteric modulators can reshape GPCR conformational landscapes.

To further delineate the PP-001 binding site, we generated NTSR1 constructs containing sequential alanine substitutions in the ICL1-3 and C-terminal domains and assessed their responses to NT(8-13) and PP-001 in radioligand binding assays. Although PP-001's inhibitory activity on NT binding was largely preserved, selected mutations in ICL1, ICL3, and the C-terminal domains, particularly those encompassing or adjacent to H8, caused rightward shifts in potency. This finding parallels the work of Zhang et al.[121], who proposed that the PAR1-derived pepducin P1pal-19 binds to H8 in a manner analogous to the second protomer in a PAR1−PAR1 dimer, as deletion of H8 abolished pepducin−receptor interactions. Similarly, Sevigny et al.[9] exploited the ICL3-H8 interface of PAR2 to design potent antagonist pepducins. Despite key differences (PP-001 being derived from ICL1 and displaying signaling bias and NAM properties, whereas P1pal-19 is an ICL3-derived allosteric agonist), both pepducins appear to interact with H8 to modulate 7TMR function. Interestingly, conformational rearrangements in H8 have been shown to govern the biased G-protein activation of the mu-opioid receptor (MOR)[124], a feature mirrored by PP-001'activity profile. Finally, molecular docking of PP-001 to an NT(8−13)-bound, membrane-equilibrated NTSR1 structure revealed interactions spanning the TM7-H8 bend and the ICL1/ICL3 interface. By engaging the amphipathic H8 and its hinge region, PP-001 appears to stabilize receptor states compatible with G-protein coupling while partially encroaching on the binding interface. Together, these docking and mutagenesis data provide a coherent structural rationale for the experimentally observed combination of decreased orthosteric affinity, reduced signaling, and preserved G-protein-biased activity.

4.1. Limitations of this study

An important qualification should be noted. The thermostability assays were performed using rat NTSR1−3 and NTSR1−22 constructs, whereas the ICL mutant series was generated from human NTSR1. Although rat and human NTSR1 share 84% sequence identity and an identical ICL1 sequence, species-specific differences may still influence the PP-001 binding mode. Moreover, while the rNTSR1−3 construct retains all residues corresponding to the substitutions in Mutants 2, 16, 17, 19, and 20, this is not the case for rNTSR1−22. In this construct, H305 (Mutant 16) is replaced by arginine, and the sequences encompassing V372-S373 (Mutant 17) and the entire regions (V372 to Y424) corresponding to Mutants 19 and 20 are deleted. Remarkably, despite the loss of these sites, PP-001 binding to rNTSR1−22 was still observed. These findings suggest that while our radioligand binding data highlight H8 as a key determinant for PP-001 interaction, the binding site likely spans multiple intracellular domains, including ICL1 and ICL3 (as implicated by Mutants 2 and 16) and potentially other domains for which data were unavailable (Mutants 1, 4, 5, 8, or 18). It is also possible that our alanine scan strategy, substituting residues in blocks of five, may have obscured critical residues located at the junctions between mutant segments. Notably, even in Mutant 19, which showed the largest rightward shift in PP-001 potency, NT binding was still fully inhibited at 100 μmol/L, indicating that partial PP-001 binding was retained.

In summary, these results underscore the complexity of the PP-001/NTSR1 interaction, in which the pepducin acts as both a G protein-biased intracellular allosteric agonist and a negative allosteric modulator of NT function. This dual activity distinguishes PP-001 from small molecule intracellular NTSR1 modulators, such as ML314, SBI-553, which instead promote-biased signaling and function as positive allosteric modulators (PAMs) of NT-mediated responses[114,117,125]. NTSR1-derived pepducins, therefore offer a unique pharmacological framework for exploring the conformational and signaling diversity of GPCRs and may inform the design of next-generation therapeutics.

Acknowledgments

This study was supported by Canadian Institutes of Health Research grant FDN-148413, Fonds de recherche du Québec − Nature et technologies (FRQ-NT) grant 2018-PR-207951. The authors would like to thank Drs. Bouvier M, Hébert T, Laporte SA, Pineyro G, Leduc R, Tardif JC, and Thorin E for providing us with BRET-based biosensors. Rebbeca L. Brouillette is the recipient of Ph.D. scholarships from the Fonds de recherche du Québec − Santé (FRQ-S) and the Canadian Institutes of Health Research (CIHR). Frédérique Lussier is a recipient of a Master's-level scholarship from the CIHR, Émile Breault is a recipient of Master's-level scholarships from the FRQ-S and the CIHR. Élie Besserer-Offroy is the recipient of an Excellence Research Chair in Innovative Theranostic Approaches in Ovarian Cancers (THERANOVCA) funded by the Region Normandie and cofunded by the European Union. Philippe Sarret is the recipient of a Tier 1 Canada Research Chair in Neurophysiopharmacology of Chronic Pain and a member of the FRQ-S-funded Quebec Pain Research Network (QPRN).

Author contribution

Conceptualization: Christine E. Mona, Élie Besserer-Offroy, and Philippe Sarret. Formal analysis: Rebbeca L. Brouillette, Malihe Hassanzadeh, and Véronique Blais. Funding acquisition: Christine E. Mona, Michel Grandbois, Élie Besserer-Offroy, and Philippe Sarret. Investigation: Rebbeca L. Brouillette, Émile Breault, Frédérique Lussier, Nathan Meneboo, Malihe Hassanzadeh, Victoria Tremblay, Laurence Ulrich, Magali Chartier, Jérôme Côté, and Véronique Blais. Methodology: Rebbeca L. Brouillette, Christine E. Mona, and Élie Besserer-Offroy. Project administration: Jean-Michel Longpré, Michel Grandbois, Pierre-Luc Boudreault, Martin Audet, Élie Besserer-Offroy, and Philippe Sarret. Resources: Élora Midavaine. Supervision: Élie Besserer-Offroy and Philippe Sarret. Visualization: Rebbeca L.Brouillette, Malihe Hassanzadeh, and Véronique Blais. Writing − original draft, Rebecca L. Brouillette. Writing − review & editing, Jean-Michel Longpré, Michel Grandbois, Élie Besserer-Offroy, and Philippe Sarret.

Conflicts of interest

The authors declare no competing financial interests.

Data and materials availability

The BRET^2 constructs Gα_q-RlucII, Gα_{i1}-RlucII, Gα_{oA}-RlucII, Gα_{13}-RlucII, GFP10-Gγ_1, RlucII-β-arrestin-1, RlucII-β-arrestin-2, and rGFP-CAAX were available to us through a materials transfer agreement (MTA) with Dr. Michel Bouvier's laboratory (Université de Montréal). All data are available in the main text or in the Supporting Information

Appendix A. Supporting information

Supporting information to this article can be found online at https://doi.org/10.1016/j.apsb.2025.12.043.

References

1. Covic L, Gresser AL, Talavera J, Swift S, Kuliopulos A. Activation and inhibition of G protein-coupled receptors by cell-penetrating membrane-tethered peptides. *Proc Natl Acad Sci* 2002;**99**:643−8.
2. Wielders SJH, Bennaghmouch A, Reutelingsperger CPM, Bevers EM, Lindhout T. Anticoagulant and antithrombotic properties of intracellular protease-activated receptor antagonists. *J Thromb Haemostasis* 2007;**5**:571−6.
3. Tsuji M, Ueda S, Hirayama T, Okuda K, Sakaguchi Y, Isono A, et al. FRET-based imaging of transbilayer movement of pepducin in living cells by novel intracellular bioreductively activatable fluorescent probes. *Org Biomol Chem* 2013;**11**:3030.
4. Janz JM, Ren Y, Looby R, Kazmi MA, Sachdev P, Grunbeck A, et al. Direct interaction between an allosteric agonist pepducin and the chemokine receptor CXCR4. *J Am Chem Soc* 2011;**133**:15878−81.
5. Tchernychev B, Ren Y, Sachdev P, Janz JM, Haggis L, O'Shea A, et al. Discovery of a CXCR4 agonist pepducin that mobilizes bone marrow hematopoietic cells. *Proc Natl Acad Sci* 2010;**107**:22255−9.
6. Carr R, Du Y, Quoyer J, Panettieri RA, Janz JM, Bouvier M, et al. Development and characterization of pepducins as Gs-biased allosteric agonists. *J Biol Chem* 2014;**289**:35668−84.
7. Carr R, Schilling J, Song J, Carter RL, Du Y, Yoo SM, et al. β-Arrestin−biased signaling through the β_2-adrenergic receptor promotes cardiomyocyte contraction. *Proc Natl Acad Sci* 2016;**113**: E4107−16.
8. Cisowski J, O'Callaghan K, Kuliopulos A, Yang J, Nguyen N, Deng Q, et al. Targeting protease-activated receptor-1 with cell-penetrating pepducins in lung cancer. *Am J Pathol* 2011;**179**:513−23.
9. Sevigny LM, Zhang P, Bohm A, Lazarides K, Perides G, Covic L, et al. Interdicting protease-activated receptor-2-driven inflammation with cell-penetrating pepducins. *Proc Natl Acad Sci* 2011;**108**: 8491−6.
10. Lee SK, Malik RA, Zhou J, Wang W, Gross PL, Weitz JI, et al. PAR4 inhibition reduces coronary artery atherosclerosis and myocardial fibrosis in SR-B1/LDLR double knockout mice. *Arterioscler Thromb Vasc Biol* 2023;**43**:2165−78.
11. Severino B, Incisivo GM, Fiorino F, Bertolino A, Frecentese F, Barbato F, et al. Identification of a pepducin acting as $S1P_3$ receptor antagonist: pepducin acting as $S1P_3$ receptor antagonist. *J Pept Sci* 2013;**19**:717−24.
12. Corvino A, Cerqua I, Lo Bianco A, Caliendo G, Fiorino F, Frecentese F, et al. Antagonizing S1P3 receptor with cell-penetrating pepducins in skeletal muscle fibrosis. *Int J Mol Sci* 2021;**22**:8861.
13. Quoyer J, Janz JM, Luo J, Ren Y, Armando S, Lukashova V, et al. Pepducin targeting the C-X-C chemokine receptor type 4 acts as a biased agonist favoring activation of the inhibitory G protein. *Proc Natl Acad Sci* 2013;**110**:E5088−9.
14. Carr R, Benovic JL. From biased signalling to polypharmacology: unlocking unique intracellular signalling using pepducins. *Biochem Soc Trans* 2016;**44**:555−61.
15. Covic L, Misra M, Badar J, Singh C, Kuliopulos A. Pepducin-based intervention of thrombin-receptor signaling and systemic platelet activation. *Nat Med* 2002;**8**:1161−5.
16. Midavaine É, Brouillette RL, Théberge E, Mona CE, Kashem SW, Côté J, et al. Discovery of a CCR2-targeting pepducin therapy for chronic pain. *Pharmacol Res* 2024;**205**:107242.
17. Kaneider NC, Agarwal A, Leger AJ, Kuliopulos A. Reversing systemic inflammatory response syndrome with chemokine receptor pepducins. *Nat Med* 2005;**11**:661−5.
18. Agarwal A, Tressel SL, Kaimal R, Balla M, Lam FH, Covic L, et al. Identification of a metalloprotease-chemokine signaling system in the ovarian cancer microenvironment: implications for anti-angiogenic therapy. *Cancer Res* 2010;**70**:5880−90.
19. Winther M, Gabl M, Welin A, Dahlgren C, Forsman H. A neutrophil inhibitory pepducin derived from FPR1 expected to target FPR1 signaling hijacks the closely related FPR2 instead. *FEBS Lett* 2015; **589**:1832−9.
20. Forsman H, Bylund J, Oprea TI, Karlsson A, Boulay F, Rabiet MJ, et al. The leukocyte chemotactic receptor FPR2, but not the closely related FPR1, is sensitive to cell-penetrating pepducins with amino acid sequences descending from the third intracellular receptor loop. *Biochim Biophys Acta BBA - Mol Cell Res* 2013;**1833**:1914−23.
21. Gabl M, Winther M, Skovbakke SL, Bylund J, Dahlgren C, Forsman H. A pepducin derived from the third intracellular loop of FPR2 is a partial agonist for direct activation of this receptor in neutrophils but a full agonist for cross-talk triggered reactivation of FPR2. *PLoS One* 2014;**9**:e109516.
22. Lee HY, Kim HS, Jeong YS, Kim JC, Bae YS, Jo YH, et al. A membrane-tethering pepducin derived from formyl peptide receptor 3 shows strong therapeutic effects against sepsis. *Biochem Biophys Res Commun* 2020;**524**:156−62.
23. Licht T, Tsirulnikov L, Reuveni H, Yarnitzky T, Ben-Sasson SA. Induction of pro-angiogenic signaling by a synthetic peptide derived from the second intracellular loop of S1P3 (EDG3). *Blood* 2003;**102**: 2099−107.
24. Nassour H, Hoang TA, Martin RD, Dallagnol JCC, Billard É, Létourneau M, et al. Lipidated peptides derived from intracellular loops 2 and 3 of the urotensin II receptor act as biased allosteric ligands. *J Biol Chem* 2021;**297**:101057.
25. O'Brien MS, McDougall JJ. Targeting proteinase activated receptor-4 reduces mechanonociception during the acute inflammatory phase but not the chronic neuropathic phase of osteoarthritis in rats. *Front Pharmacol* 2021;**12**:756632.
26. Boire A, Covic L, Agarwal A, Jacques S, Sherifi S, Kuliopulos A. PAR1 is a matrix metalloprotease-1 receptor that promotes invasion and tumorigenesis of breast cancercells. *Cell* 2005;**120**:303−13.
27. Jamieson T, Clarke M, Steele CW, Samuel MS, Neumann J, Jung A, et al. Inhibition of CXCR2 profoundly suppresses inflammation-driven and spontaneous tumorigenesis. *J Clin Investig* 2012;**122**: 3127−44.
28. Pagano E, Elias JE, Schneditz G, Saveljeva S, Holland LM, Borrelli F, et al. Activation of the GPR35 pathway drives angiogenesis in the tumour microenvironment. *Gut* 2022;**71**:509−20.
29. Jiang Y, Zhuo X, Wu Y, Fu X, Mao C. PAR2 blockade reverses osimertinib resistance in non-small-cell lung cancer cells *via* attenuating ERK-mediated EMT and PD-L1 expression. *Biochim Biophys Acta BBA - Mol Cell Res* 2022;**1869**:119144.
30. Agarwal A, Covic L, Sevigny LM, Kaneider NC, Lazarides K, Azabdaftari G, et al. Targeting a metalloprotease-PAR1 signaling system with cell-penetrating pepducins inhibits angiogenesis, ascites, and progression of ovarian cancer. *Mol Cancer Therapeut* 2008;**7**: 2746−57.
31. Armstrong CWD, Coulter JA, Ong CW, Maxwell PJ, Walker S, Butterworth KT, et al. Clinical and functional characterization of CXCR1/CXCR2 biology in the relapse and radiotherapy resistance of primary PTEN-deficient prostate carcinoma. *NAR Cancer* 2020;**2**. zcaa012.
32. O'Callaghan K, Lee L, Nguyen N, Hsieh MY, Kaneider NC, Klein AK, et al. Targeting CXCR4 with cell-penetrating pepducins in lymphoma and lymphocytic leukemia. *Blood* 2012;**119**:1717−25.
33. Fletcher EK, Ngwenyama N, Nguyen N, Turner SE, Covic L, Alcaide P, et al. Suppression of heart failure with PAR1 pepducin technology in a pressure overload model in mice. *Circ Heart Fail* 2023;**16**:e010621.
34. Barr TP, Garzia C, Guha S, Fletcher EK, Nguyen N, Wieschhaus AJ, et al. PAR2 pepducin-based suppression of inflammation and itch in atopic dermatitis models. *J Invest Dermatol* 2019;**139**:412−21.
35. Patricio ES, Costa R, Figueiredo CP, Gers-Barlag K, Bicca MA, Manjavachi MN, et al. Mechanisms underlying the scratching

behavior induced by the activation of proteinase-activated receptor-4 in mice. *J Invest Dermatol* 2015;**135**:2484−91.
36. Cheng J, Yang Z, Ge XY, Gao MX, Meng R, Xu X, et al. Autonomous sensing of the insulin peptide by an olfactory G protein-coupled receptor modulates glucose metabolism. *Cell Metab* 2022; **34**:240−255.e10.
37. Luyendyk JP, Mackman N, Sullivan BP. Role of fibrinogen and protease-activated receptors in acute xenobiotic-induced cholestatic liver injury. *Toxicol Sci* 2011;**119**:233−43.
38. Kaneider NC, Leger AJ, Agarwal A, Nguyen N, Perides G, Derian C, et al. "Role reversal" for the receptor PAR1 in sepsis-induced vascular damage. *Nat Immunol* 2007;**8**:1303−12.
39. Kuliopulos A, Gurbel PA, Rade JJ, Kimmelstiel CD, Turner SE, Bliden KP, et al. PAR1 (protease-activated receptor 1) pepducin therapy targeting myocardial necrosis in coronary artery disease and acute coronary syndrome patients undergoing cardiac catheterization: a randomized, placebo-controlled, phase 2 study. *Arterioscler Thromb Vasc Biol* 2020;**40**:2990−3003.
40. Zhang P, Gruber A, Kasuda S, Kimmelstiel C, O'Callaghan K, Cox DH, et al. Suppression of arterial thrombosis without affecting hemostatic parameters with a cell-penetrating PAR1 pepducin. *Circulation* 2012;**126**:83−91.
41. Gurbel PA, Bliden KP, Turner SE, Tantry US, Gesheff MG, Barr TP, et al. Cell-penetrating pepducin therapy targeting PAR1 in subjects with coronary artery disease. *Arterioscler Thromb Vasc Biol* 2016;**36**: 189−97.
42. Brouillette RL, Besserer-Offroy É, Mona CE, Chartier M, Lavenus S, Sousbie M, et al. Cell-penetrating pepducins targeting the neurotensin receptor type 1 relieve pain. *Pharmacol Res* 2020;**155**:104750.
43. Roussy G, Dansereau MA, Doré-Savard L, Belleville K, Beaudet N, Richelson E, et al. Spinal NTS1 receptors regulate nociceptive signaling in a rat formalin tonic pain model. *J Neurochem* 2008;**105**: 1100−14.
44. Azriel Y, Burcher E. Characterization and autoradiographic localization of neurotensin binding sites in human sigmoid colon. *J Pharmacol Exp Therapeut* 2001;**297**:1074−81.
45. Schaeffer P, Laplace MC, Savi P, Pflieger AM, Gully D, Herbert JM. Human umbilical vein endothelial cells express high affinity neurotensin receptors coupled to intracellular calcium release. *J Biol Chem* 1995;**270**:3409−13.
46. Rioux F, Quirion R, Kérouac R, St-Pierre S. The pressor effects of neurotensin and related peptides in rats. *Neuropeptides* 1982;**2**: 295−9.
47. Feifel D, Goldenberg J, Melendez G, Shilling PD. The acute and subchronic effects of a brain-penetrating, neurotensin-1 receptor agonist on feeding, body weight and temperature. *Neuropharmacology* 2010;**58**:195−8.
48. Guo R, Chen O, Zhou Y, Bang S, Chandra S, Li Y, et al. Arrestin-biased allosteric modulator of neurotensin receptor 1 alleviates acute and chronic pain. *Cell* 2025;**188**:4332−4349.e21.
49. Nemeroff CB, Osbahr AJ, Manberg PJ, Ervin GN, Prange AJ. Alterations in nociception and body temperature after intracisternal administration of neurotensin, beta-endorphin, other endogenous peptides, and morphine. *Proc Natl Acad Sci U S A* 1979;**76**:5368−71.
50. Guillemette A, Dansereau MA, Beaudet N, Richelson E, Sarret P. Intrathecal administration of NTS1 agonists reverses nociceptive behaviors in a rat model of neuropathic pain: intrathecal administration of NTS1 agonists reverses nociceptive behaviors in a rat model of neuropathic pain. *Eur J Pain* 2012;**16**:473−84.
51. Breton B, Sauvageau É, Zhou J, Bonin H, Le Gouill C, Bouvier M. Multiplexing of multicolor bioluminescence resonance energy transfer. *Biophys J* 2010;**99**:4037−46.
52. Galés C, Van Durm JJJ, Schaak S, Pontier S, Percherancier Y, Audet M, et al. Probing the activation-promoted structural rearrangements in preassembled receptor-G protein complexes. *Nat Struct Mol Biol* 2006;**13**:778−86.
53. Richard-Lalonde M, Nagi K, Audet N, Sleno R, Amraei M, Hogue M, et al. Conformational dynamics of Kir3.1/Kir3.2 channel activation *via* δ-opioid receptors. *Mol Pharmacol* 2013;**83**:416−28.
54. Demeule M, Beaudet N, Régina A, Besserer-Offroy É, Murza A, Tétreault P, et al. Conjugation of a brain-penetrant peptide with neurotensin provides antinociceptive properties. *J Clin Investig* 2014; **124**:1199−213.
55. Galés C, Rebois RV, Hogue M, Trieu P, Breit A, Hébert TE, et al. Real-time monitoring of receptor and G-protein interactions in living cells. *Nat Methods* 2005;**2**:177−84.
56. Armando S, Quoyer J, Lukashova V, Maiga A, Percherancier Y, Heveker N, et al. The chemokine CXC4 and CC2 receptors form homo- and heterooligomers that can engage their signaling G-protein effectors and estin. *FASEB J Off Publ Fed Am Soc Exp Biol* 2014;**28**: 4509−23.
57. Zimmerman B, Beautrait A, Aguila B, Charles R, Escher E, Claing A, et al. Differential β-arrestin-dependent conformational signaling and cellular responses revealed by angiotensin analogs. *Sci Signal* 2012;**5**. ra33.
58. Paradis JS, Ly S, Blondel-Tepaz É, Galan JA, Beautrait A, Scott MGH, et al. Receptor sequestration in response to β-arrestin-2 phosphorylation by ERK1/2 governs steady-state levels of GPCR cell-surface expression. *Proc Natl Acad Sci U S A* 2015;**112**: E5160−8.
59. Namkung Y, Le Gouill C, Lukashova V, Kobayashi H, Hogue M, Khoury E, et al. Monitoring G protein-coupled receptor and β-arrestin trafficking in live cells using enhanced bystander BRET. *Nat Commun* 2016;**7**:12178.
60. Besserer-Offroy É, Brouillette RL, Lavenus S, Froehlich U, Brumwell A, Murza A, et al. The signaling signature of the neurotensin type 1 receptor with endogenous ligands. *Eur J Pharmacol* 2017;**805**:1−13.
61. Besserer-Offroy É, Bérubé P, Côté J, Murza A, Longpré JM, Dumaine R, et al. The hypotensive effect of activated apelin receptor is correlated with β-arrestin recruitment. *Pharmacol Res* 2018;**131**: 7−16.
62. Deluigi M, Klipp A, Klenk C, Merklinger L, Eberle SA, Morstein L, et al. Complexes of the neurotensin receptor 1 with small-molecule ligands reveal structural determinants of full, partial, and inverse agonism. *Sci Adv* 2021;**7**. eabe5504.
63. Krumm BE, White JF, Shah P, Grisshammer R. Structural prerequisites for G-protein activation by the neurotensin receptor. *Nat Commun* 2015;**6**:7895.
64. Ehrhardt C, Schmolke M, Matzke A, Knoblauch A, Will C, Wixler V, et al. Polyethylenimine, a cost-effective transfection reagent. *Signal Transduct* 2006;**6**:179−84.
65. Kroeze WK, Sassano MF, Huang XP, Lansu K, McCorvy JD, Giguère PM, et al. PRESTO-Tango as an open-source resource for interrogation of the druggable human GPCRome. *Nat Struct Mol Biol* 2015;**22**:362−9.
66. Alexandrov AI, Mileni M, Chien EYT, Hanson MA, Stevens RC. Microscale fluorescent thermal stability assay for membrane proteins. *Structure* 2008;**16**:351−9.
67. Berman HM, Westbrook J, Feng Z, Gilliland G, Bhat TN, Weissig H, et al. The protein data bank. *Nucleic Acids Res* 2000;**28**:235−42.
68. Jo S, Kim T, Iyer VG, Im W. CHARMM-GUI: a web-based graphical user interface for CHARMM. *J Comput Chem* 2008;**29**:1859−65.
69. Abraham MJ, Murtola T, Schulz R, Páll S, Smith JC, Hess B, et al. GROMACS: high performance molecular simulations through multi-level parallelism from laptops to supercomputers. *SoftwareX* 2015; **1**−**2**:19−25.
70. Lee J, Cheng X, Swails JM, Yeom MS, Eastman PK, Lemkul JA, et al. CHARMM-GUI input generator for NAMD, GROMACS, AMBER, OpenMM, and CHARMM/OpenMM simulations using the CHARMM36 additive force field. *J Chem Theor Comput* 2016;**12**: 405−13.

71. Hess B, Bekker H, Berendsen HJC, Fraaije JGEM. LINCS: a linear constraint solver for molecular simulations. *J Comput Chem* 1997; **18**:1463−72.
72. Huang J, Rauscher S, Nawrocki G, Ran T, Feig M, de Groot BL, et al. CHARMM36m: an improved force field for folded and intrinsically disordered proteins. *Nat Methods* 2017;**14**:71−3.
73. Darden T, York D, Pedersen L. Particle mesh Ewald: an N•log(N) method for Ewald sums in large systems. *J Chem Phys* 1993;**98**: 10089−92.
74. Essmann U, Perera L, Berkowitz ML, Darden T, Lee H, Pedersen LG. A smooth particle mesh Ewald method. *J Chem Phys* 1995;**103**:8577−93.
75. Bussi G, Donadio D, Parrinello M. Canonical sampling through velocity rescaling. *J Chem Phys* 2007;**126**:014101.
76. Bernetti M, Bussi G. Pressure control using stochastic cell rescaling. *J Chem Phys* 2020;**153**:114107.
77. Jorgensen WL, Chandrasekhar J, Madura JD, Impey RW, Klein ML. Comparison of simple potential functions for simulating liquid water. *J Chem Phys* 1983;**79**:926−35.
78. Baek M, Anishchenko I, Humphreys IR, Cong Q, Baker D, DiMaio F. Efficient and accurate prediction of protein structure using RoseTTAFold2 2023. *bioRxiv* 2023. Available from: https://doi.org/10.1101/2023.05.24.542179.
79. Steinegger M, Söding J. MMseqs2 enables sensitive protein sequence searching for the analysis of massive data sets. *Nat Biotechnol* 2017; **35**:1026−8.
80. Labute P. The generalized Born/volume integral implicit solvent model: estimation of the free energy of hydration using London dispersion instead of atomic surface area. *J Comput Chem* 2008;**29**: 1693−8.
81. St-Pierre S, Lalonde JM, Gendreau M, Quirion R, Regoli D, Rioux F. Synthesis of peptides by the solid-phase method. 6. Neurotensin, fragments, and analogs. *J Med Chem* 1981;**24**:370−6.
82. Griffin MT, Figueroa KW, Liller S, Ehlert FJ. Estimation of agonist activity at G protein-coupled receptors: analysis of M_2 muscarinic receptor signaling through $G_{i/o}$,G_s , and G_{15}. *J Pharmacol Exp Therapeut* 2007;**321**:1193−207.
83. Rajagopal S, Ahn S, Rominger DH, Gowen-MacDonald W, Lam CM, DeWire SM, et al. Quantifying ligand bias at seven-transmembrane receptors. *Mol Pharmacol* 2011;**80**:367−77.
84. Kenakin T, Watson C, Muniz-Medina V, Christopoulos A, Novick S. A simple method for quantifying functional selectivity and agonist bias. *ACS Chem Neurosci* 2012;**3**:193−203.
85. Black JW, Leff P. Operational models of pharmacological agonism. *Proc R Soc Lond B Biol Sci* 1983;**220**:141−62.
86. Shpakov AO. Allosteric regulation of G-protein-coupled receptors: from diversity of molecular mechanisms to multiple allosteric sites and their ligands. *Int J Mol Sci* 2023;**24**:6187.
87. Oakley RH, Laporte SA, Holt JA, Caron MG, Barak LS. Differential affinities of visual arrestin, βArrestin1, and βArrestin2 for G protein-coupled receptors delineate two major classes of receptors. *J Biol Chem* 2000;**275**:17201−10.
88. Oakley RH, Laporte SA, Holt JA, Barak LS, Caron MG. Molecular determinants underlying the formation of stable intracellular G protein-coupled receptor-β-Arrestin complexes after receptor endocytosis. *J Biol Chem* 2001;**276**:19452−60.
89. Savdie C, Ferguson SSG, Vincent JP, Beaudet A, Stroh T. Cell-type-specific pathways of neurotensin endocytosis. *Cell Tissue Res* 2006; **324**:69−85.
90. Bourque K, Jones-Tabah J, Devost D, Clarke PBS, Hébert TE. Exploring functional consequences of GPCR oligomerization requires a different lens. *Prog Mol Biol Transl Sci* 2020;**169**: 181−211.
91. White JF, Grodnitzky J, Louis JM, Trinh LB, Shiloach J, Gutierrez J, et al. Dimerization of the class A G protein-coupled neurotensin receptor NTS1 alters G protein interaction. *Proc Natl Acad Sci* 2007; **104**:12199−204.
92. Harding PJ, Attrill H, Boehringer J, Ross S, Wadhams GH, Smith E, et al. Constitutive dimerization of the G-protein coupled receptor, neurotensin receptor 1, reconstituted into phospholipid bilayers. *Biophys J* 2009;**96**:964−73.
93. Hwang JR, Baek MW, Sim J, Choi HS, Han JM, Kim YL, et al. Intermolecular cross-talk between NTR1 and NTR2 neurotensin receptor promotes intracellular sequestration and functional inhibition of NTR1 receptors. *Biochem Biophys Res Commun* 2010;**391**: 1007−13.
94. Dijkman PM, Castell OK, Goddard AD, Munoz-Garcia JC, De Graaf C, Wallace MI, et al. Dynamic tuneable G protein-coupled receptor monomer-dimer populations. *Nat Commun* 2018;**9**:1710.
95. Marullo S, Bouvier M. Resonance energy transfer approaches in molecular pharmacology and beyond. *Trends Pharmacol Sci* 2007;**28**: 362−5.
96. Perron A, Sharif N, Sarret P, Stroh T, Beaudet A. NTS2 modulates the intracellular distribution and trafficking of NTS1 *via* heterodimerization. *Biochem Biophys Res Commun* 2007;**353**: 582−90.
97. Koschatzky S, Tschammer N, Gmeiner P. Cross-receptor interactions between dopamine D_{2L} and neurotensin NTS_1 receptors modulate binding affinities of dopaminergics. *ACS Chem Neurosci* 2011;**2**: 308−16.
98. Borroto-Escuela DO, Ravani A, Tarakanov AO, Brito I, Narvaez M, Romero-Fernandez W, et al. Dopamine D2 receptor signaling dynamics of dopamine D2-neurotensin 1 receptor heteromers. *Biochem Biophys Res Commun* 2013;**435**:140−6.
99. Liu H, Tian Y, Ji B, Lu H, Xin Q, Jiang Y, et al. Heterodimerization of the kappa opioid receptor and neurotensin receptor 1 contributes to a novel β-arrestin-2-biased pathway. *Biochim Biophys Acta BBA-Mol Cell Res* 2016;**1863**:2719−38.
100. Bai B, Cai X, Jiang Y, Karteris E, Chen J. Heterodimerization of apelin receptor and neurotensin receptor 1 induces phosphorylation of $ERK_{1/2}$ and cell proliferation *via* Gαq-mediated mechanism. *J Cell Mol Med* 2014;**18**:2071−81.
101. Carraway R, Leeman SE. The isolation of a new hypotensive peptide, neurotensin, from bovine hypothalami. *J Biol Chem* 1973;**248**: 6854−61.
102. Chalon P, Vita N, Kaghad M, Guillemot M, Bonnin J, Delpech B, et al. Molecular cloning of a levocabastine-sensitive neurotensin binding site. *FEBS Lett* 1996;**386**:91−4.
103. Vita N, Laurent P, Lefort S, Chalon P, Dumont X, Kaghad M, et al. Cloning and expression of a complementary DNA encoding a high affinity human neurotensin receptor. *FEBS Lett* 1993;**317**:139−42.
104. Gully D, Lespy L, Canton M, Rostene W, Kitabgi P. Effect of the neurotensin receptor antagonist SR48692 on rat blood pressure modulation by neurotensin. *Life Sci* 1996;**58**:665−74.
105. Schaeffer P, Laplace MC, Prabonnaud V, Bernat A, Gully D, Lespy L, et al. Neurotensin induces the release of prostacyclin from human umbilical vein endothelial cells *in vitro* and increases plasma prostacyclin levels in the rat. *Eur J Pharmacol* 1997;**323**:215−21.
106. Halai R, Cooper MA. Using label-free screening technology to improve efficiency in drug discovery. *Expet Opin Drug Discov* 2012;**7**: 123−31.
107. Sampson CDD, Bellavista CF, Stewart MJ, Mulligan C. Thermostability-based binding assays reveal complex interplay of cation, substrate and lipid binding in the bacterial DASS transporter, VcINDY. *Biochem J* 2021;**478**:3847−67.
108. Holdfeldt A, Lind S, Hesse C, Dahlgren C, Forsman H. The PAR4-derived pepducin P4Pal10 lacks effect on neutrophil GPCRs that couple to Gαq for signaling but distinctly modulates function of the Gαi-coupled FPR2 and FFAR2. *Biochem Pharmacol* 2020;**180**: 114143.

109. Kenakin TP. Biased signalling and allosteric machines: new vistas and challenges for drug discovery: 7TMRs as allosteric proteins. *Br J Pharmacol* 2012;**165**:1659−69.
110. Kenakin T. Allostery: the good, the bad, and the ugly. *J Pharmacol Exp Therapeut* 2024;**388**:110−20.
111. Fantegrossi WE, Ko MCH, Woods JH, Richelson E. Antinociceptive, hypothermic, hypotensive, and reinforcing effects of a novel neurotensin receptor agonist, NT69L, in rhesus monkeys. *Pharmacol Biochem Behav* 2005;**80**:341−9.
112. Oishi M, Inagaki C, Fujiwara M, Takaori S, Yajima H, Akazawa Y. Possible mechanisms of the triphasic effects of neurotensin on the rat blood pressure. *Jpn J Pharmacol* 1981;**31**:1043−9.
113. Rioux F, Kérouac R, St-Pierre S. Analysis of the biphasic depressor-pressor effect and tachycardia caused by neurotensin in ganglion-blocked rats. *Neuropeptides* 1982;**3**:113−27.
114. Pinkerton AB, Peddibhotla S, Yamamoto F, Slosky LM, Bai Y, Maloney P, et al. Discovery of β-Arrestin biased, orally bioavailable, and CNS penetrant neurotensin receptor 1 (NTR1) allosteric modulators. *J Med Chem* 2019;**62**:8357−63.
115. Krumm BE, DiBerto JF, Olsen RHJ, Kang HJ, Slocum ST, Zhang S, et al. Neurotensin receptor allosterism revealed in complex with a biased allosteric modulator. *Biochemistry* 2023;**62**:1233−48.
116. Duan J, Liu H, Zhao F, Yuan Q, Ji Y, Cai X, et al. GPCR activation and GRK2 assembly by a biased intracellular agonist. *Nature* 2023; **620**:676−81.
117. Slosky LM, Bai Y, Toth K, Ray C, Rochelle LK, Badea A, et al. β-Arrestin-biased allosteric modulator of NTSR1 selectively attenuates addictive behaviors. *Cell* 2020;**181**:1364−1379.e14.
118. Cardenas AE, Shrestha R, Webb LJ, Elber R. Membrane permeation of a peptide: it is better to be positive. *J Phys Chem B* 2015;**119**: 6412−20.
119. Bechara C, Sagan S. Cell-penetrating peptides: 20 years later, where do we stand? *FEBS Lett* 2013;**587**:1693−702.
120. Mitchell DJ, Kim DT, Steinman L, Fathman CG, Rothbard JB. Polyarginine enters cells more efficiently than other polycationic homopolymers. *J Pept Res Off J Am Pept Soc* 2000;**56**:318−25.
121. Zhang P, Leger AJ, Baleja JD, Rana R, Corlin T, Nguyen N, et al. Allosteric activation of a G protein-coupled receptor with cell-penetrating receptor mimetics. *J Biol Chem* 2015;**290**: 15785−98.
122. Dijkman PM, Castell OK, Goddard AD, Munoz-Garcia JC, de Graaf C, Wallace MI, et al. Dynamic tuneable G protein-coupled receptor monomer-dimer populations. *Nat Commun* 2018;**9**:1710.
123. Bower JB, Robson SA, Ziarek JJ. Insights on the G protein-coupled receptor helix 8 solution structure and orientation using a neurotensin receptor 1 peptide. *Protein Sci Publ Protein Soc* 2024;**33**:e4976.
124. Cong X, Maurel D, Déméné H, Vasiliauskaité-Brooks I, Hagelberger J, Peysson F, et al. Molecular insights into the biased signaling mechanism of the μ-opioid receptor. *Mol Cell* 2021;**81**: 4165−4175.e6.
125. Hershberger P, Hedrick M, Peddibhotla S, Maloney P, Li Y, Milewski M, et al. Small molecule agonists for the neurotensin 1 receptor (NTR1 Agonists). In: *Probe reports from the NIH molecular libraries program*. Bethesda (MD): National Center for Biotechnology Information (US); 2010. 2012 Apr 8.